Geoscientific
Model Development
Discussions

Open Access

Evaluation of an operational ocean model configuration at 1/12° spatial resolution for the Indonesian seas – Part 1: Ocean physics

B. Tranchant[1], G. Reffray[2], E. Greiner[1], D. Nugroho[3,4], A. Koch-Larrouy[3], and P. Gaspar[1]

[1]CLS, Ramonville Saint-Agne, France
[2]Mercator Ocean, Ramonville Saint-Agne, France
[3]IRD/LEGOS 18 av. Ed. Belin, 31401 Toulouse, France
[4]Agency of Research and Development for Marine And Fisheries, MMAF, Jakarta, Indonesia

Correspondence to: B. Tranchant (btranchant@cls.fr)

Discussion Paper | Discussion Paper | Discussion Paper | Discussion Paper

GMDD

8, 6611–6668, 2015

Evaluation of an operational ocean model for the Indonesian seas – Part 1

B. Tranchant et al.

Title Page

Abstract | Introduction

Conclusions | References

Tables | Figures

◀ | ▶

◀ | ▶

Back | Close

Full Screen / Esc

Printer-friendly Version

Interactive Discussion

Abstract

INDO12, a 1/12° regional version of the NEMO physical ocean model covering the whole Indonesian EEZ has been developed and is now running every week in the framework of the INDESO project (Infrastructure Development of Space Oceanography) implemented by the Indonesian Ministry of Marine Affairs and Fisheries.

The initial hydrographic conditions as well as open boundary conditions are derived from the operational global ocean forecasting system at 1/4° operated by Mercator Ocean. Atmospheric forcing fields (3 hourly ECMWF analyses) are used to force the regional model. INDO12 is also forced by tidal currents and elevations, and by the inverse barometer effect. The turbulent mixing induced by internal tides is taken into account through a specific parameterization. In this study we evaluate the model skill through comparisons with various datasets including outputs of the parent model, climatologies, in situ temperature and salinity measurements, and satellite data.

The simulated and altimeter-derived Eddy Kinetic Energy fields display similar patterns and confirm that tides are a dominant forcing in the area. The volume transport of the Indonesian ThroughFlow is in good agreement with the INSTANT current meter estimates while the transport through Luzon Strait is, on average, westward but probably too weak. Significant water mass transformation occurs along the main routes of the Indonesian Throughflow (ITF) and compares well with observations. Vertical mixing is able to erode the South and North Pacific subtropical waters salinity maximum as seen in TS diagrams. Compared to satellite data, surface salinity and temperature fields display marked biases in the South China Sea.

Altogether, INDO12 proves to be able to provide a very realistic simulation of the ocean circulation and water mass transformation through the Indonesian Archipelago. A few weaknesses are also detected. Work is on-going to reduce or eliminate these problems in the second INDO12 version.

1 Introduction

INDO12, a 1/12° regional version of the NEMO physical ocean model covering the whole Indonesian EEZ has been developed and is now running every week in the framework of the INDESO project (Infrastructure Development of Space Oceanography). This project has been devised and funded by the Indonesian Ministry of Marine Affairs and Fisheries to support sustainable exploitation of Indonesian marine resources. INDESO actually includes the development of a series of coupled ocean models including a biogeochemical model and a fish population dynamics models covering three commercially important tuna species (skipjack, yellowfin and bigeye tunas). Results of the biogeochemical model are presented in a companion paper (Gutknecht et al., 2015) while simulations of tuna population dynamics will be discussed elsewhere. More details about the INDESO projects can be found at http://www.indeso.web.id.

The Indonesian archipelago is the only area where two major oceans, the Pacific and the Indian, get connected near the Equator. The complex geometry of the coastlines, the strong tides and the seasonal reversal of monsoonal winds make difficult to obtain a detailed and realistic representation of the ocean circulation.The archipelago then represents a challenge for modellers. Numerical models of the oceanic circulation through the Indonesian archipelago have been developed and prove to be rather successful. In the INDESO project, an ocean configuration at 1/12° based on the NEMO/OPA 9.0 model (Madec et al., 1998) in a fully operational way has been developed.

In this paper, we focused on the physic part. Indeed, a realistic modeling of the circulation in the Indonesian Archipelago helps to understand the role of the ITF at global scale. ITF drains water from the tropical Pacific into the Indian Ocean in a region where (i) the bottom bathymetry is complicated (see Fig. 1), (ii) numerous narrow straits and deep interior (semi-enclosed) basins up to 4000 m depth (Sulawesi, Molucca and Seram seas) exist and (iii) tidal mixing permits blending of incoming Pacific source waters into different water masses. Thus, vertical mixing within the Indone-

sian Archipelago makes substantial changes to the incoming stratified Pacific thermocline waters.

The major input of the ITF is the Mindanao Current that provides water from the upper thermocline (North Pacific Subtropical Water, NPSW) and North Pacific Intermediate Water (NPIW). This branch fills the archipelago through the Sulawesi Sea and then flows through the Makassar Strait (Gordon, 1986; Murray and Arief, 1988; Gordon and Fine, 1996). Because the Makassar strait is only 600 m depth, water below this depth are prevented to progress southward. About 80 % of the ITF transport is flowing through this shallow Makassar strait (mainly the thermocline waters), (Gordon et al., 2010). This branch of the ITF flows out of the archipelago through the Lombok Strait (about 20 % of the Makassar transport) or eventually reaches the Flores or Banda Seas to finally exits through Ombai strait or Timor Passage (Gordon and Fine, 1996).

Two secondary Eastern routes exist. One of them is taken by South Pacific Intermediate Water (SPIW) going from the South Equatorial Current (SEC) through the Maluku (or Molluca) Sea and the Lifamatola Strait into the Banda Sea and further through Ombai Strait or the Timor Passage into the Indian Ocean. Finally, the South Pacific Subtropical Water (SPSW) from the SEC takes the third route through the Halmahera and Seram Seas and eventually joins the second eastern route waters in the Banda Sea.

The fourth important path of the ITF is the flow through the SCS (South China Sea) and is referred as South China Sea Through-Flow (SCSTF). The cold and salty water inflow through the Luzon Strait becomes a warm and fresh water outflow through the Mindoro and Karimata straits, with a net volume transport 2–4 Sv (1 Sv = 10^6 m^3 s^{-1}), (see Qu et al., 2004).

The Indonesian archipelago is characterized by strong internal tides, which are trapped in the different semi-enclosed seas of the archipelago, inducing a strong mixing of water masses. Susanto et al. (2005) observed internal solitary waves generated in stratified water by interaction of successive semidiurnal tidal flows with the sill south of the Lombok strait. These waves create large vertical displacements of water masses

that are important to vertical transport and mixing of biogenic and non-biogenic components in the water column (Munk and Wunsh, 1998).

Vertical mixing within the Indonesian Seas can alter the incoming stratified Pacific thermocline waters. Salinity maximums of Pacific waters, 34.8 PSU in the North Pacific and 35.4 PSU in the South Pacific are eroded during their residence in the Indonesian seas. Finally, the ITF waters entering into the Indian Ocean are characterized by a unique water mass associated with a unique tropical stratification with a salinity of 34.6 PSU. As a result, the tropical Indian Ocean is cooled and freshened by the ITF, (Song and Gordon, 2004, 2005). Previous studies showed that vertical mixing occurs mainly in region of sharp topography such as sills or narrow straits (Ffield and Robertson, 2005; Koch-Larrouy et al., 2007). But precise locations of water mass transformations remain unclear (Koch-Larrouy et al., 2007). Different measurements of turbulent dissipation rates made during the INDOMIX 2010 cruise (Koch-Larrouy et al., 2015) could certainly help to increase our knowledge and understanding of vertical eddy diffusivity values into numerical models.

To take into account internal tidal mixing, the model explicitly solves the barotropic tides. At the resolution of the model only part of the baroclinic energy will be generated (Niwa and Hibiya, 2011). Nevertheless, how this energy will dissipate in the model remains unclear and the tidal mixing remains insufficient. To this end, an additional parameterization of tidal mixing is used to reproduce the effect of internal tide. This parameterization has especially been developed for OPA/NEMO in Indonesian seas and gives satisfying results compared to observations (Koch-Larrouy et al., 2007, 2008 2010).

This paper compares the result of the first INDESO simulation against previous results from literature detailed above in Indonesia seas. It is organized as follows. Section 2 describes the INDO12 configuration. Section 3 shows different model comparisons with different relevant dataset in the area. First, we assess INDO12 dynamics against recent scientific literature and compare meso-scale variability and tides with altimeter data and tide gauges. We compare model volume transport with transport

B. Tranchant et al.

estimates from the INSTANT campaign. Regarding the water mass transformation in the Indonesian Seas, we compare T/S diagrams of the INDO12 simulation to the parent and to observational data, such as climatology, the recent INDOMIX 2010 cruise (Koch-Larrouy et al., 2014-AGU, 2015 in revision to Deep Sea) and instantaneous data in 2013. Comparisons with satellite data such as SST from AMSR-E (The Advanced Microwave Scanning Radiometer for EOS) and SSS from Aquarius are done. We also make comparisons with monthly gridded fields combining ARGO floats (Array for Real-time Geostrophic Oceanography), Triangle Trans-Ocean Buoy Network (TRITON), and available conductivity-temperature-depth (CTD). Finally, Sect. 4 provides a summary of the results of this work by pointing out some advantages and drawbacks.

2   The INDO12 configuration

2.1   The NEMO ocean model

The regionalized configuration of the Indonesian Seas using OPA/NEMO model (Madec et al., 1998; Madec, 2008) in its NEMO2.3 version called INDO12 and developed at Mercator-Ocean is the circulation model used in the INDESO project. The regionalization configuration of the code deals with the addition of high-frequency processes such as tide and the atmospheric pressure forcing. Specific numerical schemes such as time-splitting, non-linear free surface (Levier et al., 2007) and open boundary algorithms have been implemented or improved. Specific physical parameterizations for regional modeling have been added such as GLS turbulence model including wave impact, logarithmic bottom friction, etc. In addition, the vertical mixing induced by internal tides is taken into account using the parameterization of Koch-Larrouy et al. (2007) by artificially enhancing vertical viscosity and diffusion coefficients.

This NEMO2.3 version has already been successfully applied to the IBI (Iberian-Biscay-Ireland) area (Maraldi et al., 2013). The domain covers 20° S–25° N and 90–144° E (Fig. 1) and includes the entire EEZ (Exclusive Economic Zone) of Indonesia.

The horizontal grid is an extraction of the global ORCA grid at 1/12° developed at Mercator Ocean. It is a quasi-regular grid on the Indonesian area and with a mesh approximately equal to 9 km. In the vertical direction, the model uses a partial step z coordinate (Barnier et al., 2006). The vertical grid is spread over 50 levels and a depth-dependent resolution (1 m at surface to 450 m at the bottom). In the first 10 m, the layer thickness is less than 2 m, then rise to about 10 m at 50 m deep.

The bathymetry used in this configuration is based on ETOPO2V2g (2′) and GEBCO (1′) and has been interpolated on the NEMO grid without any smoothing. Due to missing foreshore in the model, a minimal threshold value of 7 m depth has been fixed. The bathymetry has been locally modified by a hand editing mainly in the straits and passages where the sill depths have a major interest and constrain the transports. As in Metzer et al. (2010), we report sill values on Table 1 and compare to scientific literature. Note that correct sill depths are essential for proper model simulation (Gordon et al., 2003a). Without these changes, the outflow passages were quite incorrect with most of the flow going through Lombok strait instead flowing through Ombai strait and Timor passage.

2.2 External forcings

Atmospheric forcing fields come from the European center (ECMWF) and have a high frequency (3 h). "Bulk" formulae from CORE are used to model the atmosphere–ocean interface (Large and Yeager, 2004). The surface atmospheric pressure forcing is also explicitly considered.

This configuration includes explicit tidal forcing. INDO12 has geopotential tidal forcing for M2, S2, N2 and K2 (the four largest semidiurnal constituents) and for K1, O1, P1 and Q1 (the four largest diurnal constituents). As in Maraldi et al. (2013), two long-period tides Mf and Mm and one non-linear constituent (compound tides) M4 are also added. These 11 tidal constituents coming from the astronomical forcing TPX0.7 (Egbert and Erofeeva, 2002) are used to force open boundaries.

A monthly runoff climatology is built with data on coastal runoffs and 99 major rivers from Dai and Trenberth (2002) and prescribed with a flux formulation into the model. In addition, two important missing rivers (Mahakam and Kapuas on Borneo Island) with large enough rates (class 3) were added to this database.

The penetration light scheme used in this simulation is based on a 4-bands decomposition of the light. Indeed, 54 % of the solar radiation is trapped in the surface layer following an extinction depth of 0.35 m and the other part is decomposed following the red, green and blue wavelengths (Jerlov, 1968). The climatological chlorophyll values, required to calculate the absorption coefficients, were deduced from the global 1/4° input file built from the monthly SeaWifs climatological data (McClain et al., 2004).

The INDO12 simulation starts on the 03 January 2007 with conditions given by the Mercator-Ocean Global Ocean Forecasting System at 1/4° (PSY3V3R3) (Lellouche et al., 2013) started three months before from a Levitus climatology. These conditions include temperature, salinity, currents and Sea Surface Height. Open boundary conditions (OBCs) are located on a relaxation band of 10 grid points ($\sim 1°$) and come from daily output of the Global Ocean Forecasting System at 1/4°.

3 INDO12 assessment

In order to evaluate the quality of the INDO12 simulation, several diagnostics were performed on different variables such temperature, salinity and currents. Our performance analysis confronts the model results to the distinct available datasets. The first year (2007) of the simulation is considered as the model spin-up phase. Consequently, only the 2008–2013 simulated period is assessed.

3.1 The mean circulation

As noted by Ueki el al. (2003), the NGCC (New Guinea Coastal Current) exhibits a seasonal variability correlated to the monsoonal wind variation with a North-East wind

stress during the Boreal winter and a South-West wind stress during the Boreal summer. It flows northerward usually at surface and intensified during the boreal summer and southeastward during the Boreal winter (see Fig. 2). On the other hand, the New Guinea Coastal Under Current (NGCUC) flows steadily northwestward overall the year in the sub-surface thermocline layer (100–300 m) with an intensification during boreal summer (see Fig. 3).

In the Pacific region (Fig. 2), the intensity of SEC and (North Equatorial Counter Current) NECC increase during boreal winter, and are weaker during Boreal summer. The SEC and NECC are closely linked to the ITCZ (Inter Tropical Convergence Zone). They are stronger from August to December and weaker from March to May (see McPhaden et al., 1998).

Between surface and ~ 100 m depth, the seasonal variability is well represented in the major exit passages of Lombok Strait, Ombai Strait and Timor Passage with a maximum velocity (maximum transport) during the SEM (South East Monsoon) (Sprintall et al., 2009).

In the SCS, the circulation at surface is cyclonic during boreal winter and weakly anti-cyclonic during boreal summer, see (Fig. 2).

In the Indian, the Eastward surface current, the SJC (South Java Current) flows along the Indian Ocean coast of Sumatra and Java only during the NEM (North East Monsoon). During the SEM, SJC is mostly in the same direction as the westward flowing ITF (Sprintall et al., 2010), which is well reproduced in our simulation. The deeper South Java UnderCurrent (SJUC) flows also along the coast (400–800 m) in our model. It seems more clearly driven by Kelvin waves as mentioned by Sprintall et al. (2010) since it flows mainly eastward whatever the monsoon period.

3.2 EKE

In order to describe the mesoscale and eddy variability, the mean Eddy Kinetic Energy (EKE) is calculated. The EKE calculation from INOD12 simulation is performed over

the last three years (2010–2013) and compared to altimetric data (AVISO products), see Fig. 4.

Saraceno et al. (2008) point out the difficulty to represent coastal processes with conventional altimeter data due to intrinsic difficulties such as corrections applied to the altimeter data near the coast (e.g., the wet tropospheric component, high-frequency, oceanographic signals, tidal corrections, etc.). The Indonesian seas are no exception to the rule due to the presence of numerous islands and an active atmospheric convection during monsoon. In addition, in the equatorial band ($5° S$–$5° N$) the geostrophic approximation is no more valid due since the Coriolis force vanishes.

Excepted in coastal regions, EKE from INDO12 and EKE derived from altimeter data have the same strongest values at the same locations. They are localized along the Vietnam coast, near the Luzon strait (Kurushio intrusion in the SCS) and all along the Java coast (upwelling signature). In the INDO12 simulation, stronger values are found in all straits and in the main exits (Lombok, Ombai and Timor). As in Castruccio et al. (2013), large EKE values are also found within the Indonesian seas, Celebes sea, Flores Sea, Molluca sea and the southern part of the Banda Sea being the more active regions. In the Pacific, Halmahera and Mindanao eddies as well as the NGCC also show a strong signature in the EKE field.

3.3 Tides

The four primary tidal components, namely M2, S2, K1, and O1 are found to be the major components that drive tidal forcing in the Indonesian seas (Robertson and Ffield, 2008; Kartadikaria et al., 2011). In this section, we present only two primary tidal components, i.e., M2 and K1, the largest amplitude semidiurnal and diurnal constituents. Kartadikaria et al. (2011) have fully described the evolution of M2 and K1 tides in the Indonesian seas. They have shown that (i) the propagation of K1 is simpler than that of M2 component (ii) and the K1 amplitude is smaller than that of M2. Here, the K1 and M2 constituents are compared to a hydrodynamic model of the barotropic tides constrained by satellite altimetry FES2012 (Carrere et al., 2012; Stammer et al., 2014). The

INDO12 tidal sea surface elevation amplitude and phases were calculated as a complex amplitude using standard harmonic analysis applied to the sea surface height. Differences of tidal elevation between satellite altimeter data (TOPEX/POSEIDON, JASON 1 and JASON2) at crossover locations and models (INDO12 and FES2012) are shown in Fig. 5. For the M2 constituent, FES2012 is closest to the observations excepted in the SCS. On the contrary, for the K1 constituent, INDO12 is closest to the observations excepted in the SCS and along the Australian coast. Differences of tidal elevation between tides gauges (circles) and models and are also given in the same figure. Closer to the coast, the discrepancy between tide gauges and INDO12 is larger than between tide gauge and FES2012. This can be attributed to the lack of resolution along the coast in INDO12 compared to the finite element FES2012.

Figure 6 shows a power-spectrum analysis of hourly SSH from Tide gauges and from simulated moorings. As in Castruccio et al. (2012), at low frequencies, the model is in very good agreement with the observations. The spectral analysis shows that SSH fluctuations depict the same peaks at the dominant tidal frequencies, the diurnal (O1 and K1) and semidiurnal (M2 and S2). The same intensity is found in the model and in the observations. It confirms that tides are a dominant forcing in the area, and that the tidal current is dominated by the diurnal (O1 and K1) and semidiurnal (M2 and S2) frequencies. Non-linear constituents are represented by additional peaks at the higher harmonics that contain less energy in the model than the observations. As mentioned in Robertson and Ffield (2008), model errors are mainly due to a topography, stratification, resolution, and tidal forcing. Indeed, tide gauges are very close to the coast where the INDO12 model is less accurate to well represent non-linear processes. Finally, non-linear tides seems also to have more energy in the model near the East of Sumatra coast (Fig. 6a) than in the Pacific (Fig. 6c).

3.4 Volume transport (ITF and SCSTF)

The Indonesian ThroughFlow (ITF) flow along three main routes (Sprintall et al., 2004) and a good representation is given in (Gordon et al., 2012; Fig. 1).

The main western route is the flow taken by North Pacific Subtropical Water coming from the North Equatorial Current (NEC) via the Mindanao Current through the Celebes Sea, along the Makassar Strait, into the Flores Sea and the Lombok or the Ombai Strait into the Indian Ocean. In the South part of Makassar Strait, only the upper thermocline waters can flow southward into Flores and Banda seas due to the Dewakang sill (650 m).

The second path is taken by South Pacific sub-thermocline water, going from the South Equatorial Current (SEC) through the Maluku Sea and the Lifamatola Strait into the Banda Sea and further through Ombai Strait or the Timor Passage into the Indian Ocean. Lifamatola Strait, at 1940 m, regulates the flow of deep Pacific water into the interior Indonesian seas. Talley et Sprintall (2005) shows that the IIW (Intermediate Indonesian Water) attains most of its characteristics immediately downstream of Lifamatola Strait as a result of diapycnal mixing of the intermediate Pacific Ocean water masses. They also estimate a large total southward transport ($\sim$ 3 Sv). Below 1250 m, the average volume transport through Lifamatola during INSTANT (about 1.5 years between January 2004 and July 2005) was 2.5 ± 1.5 Sv (van Aken et al., 2009). It is a fairly robust number with an uncertainty of $\sim$ 5 % below 1250 m which it is not the case above 1250 m with an uncertainty that could exceed 50 % (Gordon et al., 2010). Finally, the total transport measured by INSTANT (El-Niño period) below 200 m was 1.1 Sv. In our simulation (2008–2013), the total transport is quite null and flows northward (1.6 ± 3 Sv) below 1250 m with no inter-annual variability. Above 1250 m, the net inflow is southward and varies with ENSO (El-Niño–Southern Oscillation). It is stronger during El-Niña and weaker during El-Niño. From Fig. 7, we show that the upper thermocline waters flow southward otherwise the flow is northward between 400 and 1400 m. The only deep water flowing southward is located below 1400 m with a maximum near 1700 m depth in spite of the presence of an opposite flow on the eastern side of the strait. It is a strong discrepancy with measurements and might be attributed to the bathymetry located upstream of the strait and or to open boundary conditions.

SPSW (South Pacific Subtropical Water) from the SEC takes the third route through the Halmahera and Seram Seas and joins the second route waters in the Banda Sea.

In this section, as in Sprintall et al. (2009), we consider the transport through the three major outflow passages of Lombok, Ombaï and Timor to determine the ITF transport estimates. Table 2 gives absolute values of transport in each straits and total transport for the 2008–2013 simulated period compared to INSTANT estimates (Gordon et al., 2010). Total value measured by INSTANTS (15 Sv) is stronger than in the model (12.4 Sv). This might be due to the prescribed ocean forcing fields given by the Mercator-Ocean Global Ocean Forecasting System at 1/4° (PSY3V3R3). But, INSTANT estimates and simulated INDO12 volume transports are not calculated over the same period with different ENSO signals. As we have seen before, the NW monsoon winds in boreal winter season plays an important role by weakening the total ITF volume transport. Moreover, Mayer et al., 2010 mention a blocking effect. Sprintall and Revelard (2014) argue that the 3 year time series alone is not sufficient to comprehensively resolve the interannual signal, significant transport variability during the INSTANT period was linked to ENSO and the IOD (Indian Ocean Dipole) (Sprintall et al., 2009; Gordon et al., 2008). Indeed, the INSTANT estimates reveal also inter-annual fluctuation, see Table 1 of Gordon et al. (2010). Greater ITF values are found in 2006, it is certainly due to a El-Niña event and also linked to a strong positive phase of the IOD as noted by Sprintall et al. (2009). In the INDO12 simulation, a strong inter-annual variability exists and is more or less pronounced depending on the locations and on the ENSO/IOD events (Fig. 8). In 2008 and 2013, there is no ENSO/IOD events and it gives the largest ITF transport and particularly in the Ombai and Timor straits. In 2011 and 2012, there is no ENSO event and a positive IOD, and it gives quite equivalent total transports. In 2009, the only El-Niño occurs during the simulation period and no IOD event, consequently, it is the weakest ITF transport of the period. In 2010, La Niña coincides with a negative IOD. In this case, the ITF transport is reduced with the weakest transport in Ombai and the negative IOD seems to prevail. Sprintall and Rev-

elard (2014) argue that Indian Ocean dynamics likely win out over the Pacific Ocean dynamics during concurrent ENSO and IOD events.

In order to better compare the relative transport in each of the three exit straits, we give the ratio with regard to the total mean transport volume and compare them with INSTANT estimates (Gordon et al., 2010), see Table 2.

The INDO12 simulation values for Lombok and Ombaï straits are slightly lower than the INSTANT estimates and stronger in the TIMOR passage. There is still an unbalance between Timor strait (too strong) and Ombaï strait (too weak), see also Fig. 8. In a recent paper, Oke et al. (2013) found the same kind of differences with a longer reanalysis.

The South China Sea ThroughFlow (SCSTF) affects the near surface flow in the Makassar Strait (Qu et al., 2006). It leads to the subsurface maximum in the southward current of the Makassar Strait. Gordon et al. (2003b) have shown that the intrusion of freshwater from the SCS effectively inhibits the Makassar Strait surface water from freely flowing southward. As a consequence, the Indonesian throughflow (ITF) heat transport is significantly reduced during the northeast monsoon season. The Luzon strait is the major pathway between the SCS and the Pacific Ocean. The LST (Luzon Strait Transport) is estimated to be westward and about -4 ± 5.1 Sv at 120.75° E, (Hsin et al., 2012). In the IND012 simulation, this volume transport is westward and around -0.4 Sv. Recent studies suggested different ways of improvement. Hulburt et al. (2011) shows that simulations are very sensitive to model resolution and to the accuracy of the topography and sill depths within the narrow straits in the Philippine archipelago. More recently, Zhao et al. (2014) show that the transport of the deep circulation increases with diapycnal diffusivity in the deep SCS and Luzon Strait.

3.5 Water masses transformation

In this section, we deal with the water masses transformation in the Indonesian seas. We compare INDO12 $T-S$ diagrams with WOA 2013 climatology, with parent model (PSY3) and also T/S profiles from instantaneous data (WOD 2013). $T-S$ diagrams

Full Screen / Esc

Printer-friendly Version

Interactive Discussion

comparisons are done into several sub-basins along the pathways within the Indonesian archipelago as in Koch-Larrouy et al. (2007), see Fig. 9. Model and in situ T–S diagrams are compared in the SCS and in the South Indian Ocean during several weeks in 2013.

3.5.1 Comparisons with parent model and WOA2013 climatology

Water masses from INDO12 simulation (averaged all over the period from 2008 to 2013) are compared with those of WOA 2013 climatology (Boyer et al., 2013) and with those of the parent model (PSY3V3R3) in main areas of water mass transformation, see Fig. 9.

At the main entrance, Mindanao Current drives the North Pacific water characterized by a salinity maximum (34.8 PSU), the North Pacific Subtropical Water (NPSW) and a minimum of 34.2 PSU (North Pacific Intermediate Water, NPIW). Coming from the North Pacific NPSW is saltier in the INDO12 simulation than in the WOA 2013 climatology. NPIW and the surface water are fresher (Fig. 10a).

South Pacific Subtropical Waters (SPSW) enter also into the Indonesian seas and are characterized by a salinity maximum around 35.45 PSU. Compared to the WOA 2013 climatology, SPSW in the INDO12 simulation are slightly too warm in surface and sub-surface (Fig. 10b).

Because open boundaries conditions are close to the North and South Pacific Waters, INDO12 and parent model (PSY3V3R3) differ from WOA 2013 climatology in the same way.

When comparing TS diagram in the interiors seas between the regional model that includes tidal mixing to the parent model that does not include any additional mixing, we find that the tidal mixing of the SPSW happened before entering the Banda Sea (Fig. 11). Indeed, in the Banda, Seram and Timor regions, the North and South Pacific subtropical salinity maxima are strongly attenuated in the INDO12 simulation and in better agreement than the parent simulation.

In particular the SPSW salinity maximum is strongly eroded from its entrance in the Halmahera Sea and vanishes already in the Seram Sea as noted by Koch-Larrouy et al. (2007) before. The tidal mixing strongly improves the water masses. However, there are still some biases between the climatology and the INDO12 simulation that could come from biases at the entrance of the domain.

During their residence in the Indonesian archipelago, the incoming Pacific waters are transformed to produce a unique water mass associated with a unique tropical stratification having a strong, though relatively homohaline (34.58 PSU, below 20 °C), thermocline, see T/S diagrams of Timor on Fig. 12. In the Timor and Banda regions, at the surface there is a strong freshening compared to the climatology. But comparisons do not take into account the inter-annual variability and disparities exist depending on the year (Figs. 8 and 12). This freshening is not observed at the entrance of the Indonesian domain (NPW). It is due to the Surface fresh water coming from the Java sea water that represents the major freshwater input (70 %, Koch-Larrouy et al., 2008). Moreover, a too strong freshening is observed in the model (see Sects. 3.5.3 and 3.6.1). Surface water of Makassar strait and Flores sea are lower than 33.8 PSU. It is also due to the SCS surface layer throughflow as previously shown by Gordon et al. (2012) that acts as the "fresh water plug". Note that this behavior is enhanced in 2011 (Fig. 12) when the LST is the strongest (−1.19 Sv) in the INDO12 simulation. The effect of a too strong mixing in the Banda sea (Fig. 11) can also enhance the too strong freshening at surface.

Comparing the model over a limited period to a climatology that suffer from a lack of data to properly represent inter-annual variability and regional rapid changes between each seas of the archipelago, is an imperfect exercise to validate the model. Fortunately, in the period of our simulation, the INDOMIX cruise occurs that provides unique data set to validate our model.

3.5.2 Comparisons with CTD from INDOMIX campaign

The INDOMIX cruise (July 2010, Koch-Larrouy et al., 2015) recovers in situ measurements in one of the most energetic section for internal tides through Halmahera sea and Ombai strait. Classical fine-scale CTD/LADCP measurements have been performed to-
gether with microstructure measurements at five locations, two at the entrance of the Halmahera sea (S0, S1), two in Halmahera sea (S2, S3), one in Banda sea (S4) and two (S5a/S5b) in Ombai strait (Table 3).

Koch-Larrouy et al. (2007) argued that vertical mixing due to internal tides of the SPSW occurs mainly within the Halmahera and Seram Seas before entering in the
Banda Sea.

In the following section, we compared instantaneous INDOMIX profiles (July 2010) to parent model (daily mean) and INDO12 simulation (hourly instantaneous) profiles. We see that before entering in the Halmahera sea (Fig. 13/S0), the maximum of salinity can be seen, and is in better agreement with observations in INDO12 simulation compared
to the parent model. The combined effect of the horizontal resolution and explicit tides has a crucial role. The INDO12 model exhibits a zigzag shape profile that suggests intense lateral mixing probably produces by the explicit tides.

Into the Halmahera strait (Fig. 13/S1), the maximum of salinity has already been eroded both in the observations and in the simulations. The vertical mixing seems to
be too strong in the INDO12 simulations since the mixed layer is too salty and the lower thermocline is warmer and fresher. It is in better agreement with observation than the parent model that exhibits strong salinity maximum.

At the S2 and S3 locations in the Halmahera sea (Fig. 13), T/S profiles display temperature and salinity structure with wiggles and step features in the thermocline
(more pronounced than in S1 location). Ffield and Robertson (2008) found temperature fine structure associated with straits, shallow shelves, and proximity to the shelf-slope boundary in the Indonesian seas. This phenomenon seems to be amplified during the windy JJA Southeast Monsoon time period when the upper thermocline is less strati-

fied, especially during La Nina years that which corresponds to July 2010. They associated this temperature finestructure with internal wave activity that can be a precursor to turbulent vertical mixing. The horizontal and vertical resolution of INDO12 may not able to reproduce this wave activity or they could be located slightly aside of the station
5   location.

As in S1, the mixing seems too strong since the mixed layer is too salty and the lower thermocline is warmer and fresher.

INDO12 T/S diagrams compare quite well with INDOMIX data in the Banda sea (S4). It results of mixing and advection of water masses coming from Java and Flores seas.
10 In Ombai strait (S5b), INDO12 fits very well with INDOMIX data below the pycnocline. NPIW (density 26.5) seems to be well mixed in the observations, certainly by isopycnal mixing but it is no the case in the INDO12 simulation where the NIPW signature is still present.

Finally, all T/S diagrams in the interior domain show that the parent model has defini-
15 tively not enough efficient vertical mixing and that a higher resolution model including explicit tides is needed to well mix Pacific waters in the Indonesian Archipelago.

3.5.3 Comparisons to in-situ data in the SCS (October–December 2013)

Comparisons of INDO12 simulations and WOA2009 climatology collocated with real in-situ profiles (WOD 2013) have been done in different areas during the autumn 2013.
20 These comparisons have been realized over short periods (3 months) in order to illustrate the spatial disparities of in-situ data (Fig. 14a) and the lack of in-situ data in the Indonesian Archipelago. We focus on the SCS region that is connected to the Pacific Ocean through the Luzon strait in the northern part. In the southern part of the basin, it links with the Java Sea through the Karimata Strait, and with the Sulu Sea through
25 mainly the Mindoro Strait. The fresh SCS water entering the Java Sea through the Karimata Strait inhibits the warm surface water from the Pacific flowing southward in the Makassar Strait during boreal winter (Gordon et al., 2003b; Qu et al., 2006; Tozuka et al., 2007). As the Makassar throughflow amounts to 80 % of the total ITF, the SCS ef-

fect is a major contributor to the overall variability of the ITF vertical structure. Whereas that the Karimata transport is mostly seasonal (Fang et al., 2010), circulation of the SCS demonstrates an inter-annual variation related to El Nino/Southern Oscillation (ENSO). Gordon et al. (2012) suggest the building of a "freshwater plug" in the western

5   Sulawesi Sea (via the Sibutu passage) during prolonged El Niño periods that inhibits Mindanao surface layer injection into the Makassar Strait. On the contrary, during La Nina the "freshwater plug" is dissipated which led to the entrance of surface water from the tropical Pacific Ocean.

In the Luzon strait and in the SCS (Figs. 14 and 15), the INDO12 model tends to be

10 fresher mainly at surface. This indicates that not enough Pacific waters enter into SCS and it corroborates the too weak volume transport of thermocline waters observed at Luzon strait, see 3.4. In the Luzon strait (Fig. 14), only 8 profiles are available in the southwest part of the strait. Nevertheless, the INDO12 model is able to fit one T/S profile measurement near the Philippine coast that exhibits a strong surface freshen-

15 ing occurring during October. It is not the case for the WOA 2009 climatology. For the other T/S profiles, both WOA2009 Climatology and INDO12 model are too fresh and too warm compared to observations at surface. Both measurements and model exhibit NPSW and NPIW already shown previously (Fig. 10a) and are quite close. Two T/S profiles have a too strong stratification in the INDO12 model that could be due

20 to a local too strong mixing in a region where the representation and localization of internal waves and their associated vertical mixing is still difficult to quantify. Recently Alford et al. (2015) made new measurements in the Luzon strait to better understand the formation of the world's strongest known internal waves. In the SCS, T/S profiles (Fig. 15b) shows that vertical mixing has acted by disrupting the NPSW but in a too

25 strong way by the INDO12 model.

3.6 SSS: comparisons with Aquarius and Argo monthly data

Due to the non negligible role of low salinity surface layer waters (coming from the SCS southward throughflow) on the ITF (Gordon et al., 2012), it is important to assess the SSS fields of INDO12.

3.6.1 Aquarius data

We used Aquarius Level 3[1] sea surface salinity (SSS) standard mapped image data that contains gridded 1° spatial resolution SSS averaged over one month. This particular data set is the Monthly sea surface salinity product for version 3.0 of the Aquarius data set, which is the official second release of the operational data from AQUARIUS/SAC-D mission. A summary of improvements to this new version of the Aquarius data is available.

For the previous version (V2.0), the estimated error for (monthly mean) was around 0.3–0.4 PSU (Lagerloef et al., 2013). A recent paper of Menezes et al. (2014) shows that rms difference between Aquarius (7 day Level-3 product version 2.0) with Argo is about 0.28 PSU in the tropical eastern basin of the Indian ocean [5–20° S; 90–140° E], i.e. in a region where the fresh ITF is spread westward. In addition, in a very recent paper, Tang et al. (2014) show that the monthly RMS difference with respect to Argo between 40° S and 40° N for all Aquarius SSS data products (V2.0) can be reduced to below 0.2 PSU with certain restrictions.

---

[1]*Note of Caution, RFI*: persistent negative salinity bias may be present in some regions due to RFI. Users should be very cautious with using ascending pass data in the eastern N. Atlantic and descending pass data in the western North Atlantic and *Asia Pacific region*.

3.6.2 JAMSTEC data

As in Tang et al. (2014), we use a monthly gridded data set of global oceanic salinity on 1° × 1° grid processed and delivered by the Japan Agency for Marine-Earth Science and Technology (JAMSTEC) (Hosoda et al., 2010). This product is derived from the use of the optimal interpolation (OI) method that builds the gridded fields from ARGO floats, TRITON, and available CTD.

The salinity values at 10 m depth from INDO12 are used to compare with the first level of JAMSTEC salinity at 10 dbar (∼ 10 m depth).

The advantage of the monthly Aquarius data is the spatial coverage. Monthly JAMSTEC data can not cover the Indonesian seas due to a lack of in-situ data.

3.6.3 Results

For both dataset, a negative bias exist in the Pacific region (Fig. 16) excepted near the Mindanao loop current where a positive bias exist mainly in winter and more pronounced with the Aquarius dataset. We show that the probability density function (pdf) of SSS misfit is biased (non-symetric) which corroborates the fact that processes and/or water masses into the Pacific and Indian oceans are different. Biases relative to each dataset are consistent for the same coverage. They are quite similar but stronger for Aquarius. In the Indian Ocean, a positive bias exists just after the ITF exit. It becomes negative near the Eastern Gyral Current (EGC) that flows eastward near 15° S. In the upper ocean, a strong salinity front exists between fresh water from the Indonesian Throughflow (ITF) in the South Equatorial Current (SEC) and salty subtropical waters (Menezes et al., 2013). Note also that the ITW joins the SEC and spreads westward in the Indian Ocean by advection and diffusion (Gordon et al., 1997).

Un-correlated biases near the West-Sumatra coast are located in the vicinity of many islands that could pollute the Aquarius signal. The RMSD between JAMSTEC and INDO12 in this region is higher (Fig. 17) than the RMSD between Aquarius and INDO12.

A strong negative bias (too fresh) exists in the South China Sea (SCS) which is more (in winter) or less (in summer) important depending on the season (not shown here). It could be related to an E-P bias in the ECMWF precipitation flux where the model simulation of precipitation is particularly poor over Indonesia, (see Kidd et al., 2013; Dee et al., 2011). In a recent paper, Zeng et al. (2014) argue that the smaller LST is a plausible cause of the freshening in 2012. In our model, the too strong freshening could also be due to a too weak transport at Luzon.

A positive bias exists in the South Indian Ocean excepted during April/May/June where bias tends to be negative. There is a seasonal variation of the bias into the Pacific. In the interior domain, the bias is less pronounced and there is not really a seasonal signal.

RMSD and correlations in SSS between Aquarius and INDO12 are quite similar than those between JAMSTEC and INDO12 in the pacific and Indian oceans. In the interior domain, RMSD/correlation (Fig. 17) between Aquarius and INDO12 are larger/smaller in the Java sea (monsoon variability), in the Gulf of Thailand and in the Taiwan strait (probably due to land contamination).

A region in the Indian Ocean ($95°$ E–$15°$ S) is characterized by a smaller correlation between both INDO12 and both dataset. It is certainly due to a systematic bias in the boundary conditions. This bias can be related to a lesser accuracy of MDT (Mean Dynamic Topography) (Rio et al., 2013) in the South Indian Ocean. Indeed, the MDT is involved in the process of SLA (Sea Level Anomalies) data assimilation in the parent ocean forecasting system. From Fig. 18 (left), we show that in the Indian Ocean, the three main opposite differences (statistically significant) between the two datasets (uncorrelated biases) are in the Timor sea, in the Andaman sea and on the west-coast of Sumatra. These differences can be partially explained by the salinity interpolation errors shown on Fig. 18 (right) since the maxima are found at the same locations. The Timor sea is mainly located on the continental shelf that could be explain the large interpolation errors due to the absence of ARGO floats. An uncorrelated bias exists

at the entrance of the Indonesian domain, in the Celebes sea and corresponds to the maximum of the salinity interpolation errors.

Due to the lack of JAMSTEC data in the interior domain, it is difficult to conclude on the quality of Aquarius data. Nevertheless, comparisons in the SCS (Sect. 3.5.3) have shown that the INDO12 model is fresher than the in-situ data at surface which is corroborated here with Aquarius data.

3.7   SST: comparisons to AMSR-E and Argo monthly data

The SST of the Indonesian seas is of major interest to air–sea interaction at regional and global scales see for example Sanchez et al. (2008). This is due largely to the convection process.

3.7.1   AMSR-E data

We use the SST (sea surface temperature) data retrieved from observations of the satellite microwave radiometer Advanced Microwave Scanning Radiometer on board EOS (AMSR-E). The advantage of using microwave data instead of infrared data is that the clouds influence can be neglected. For this study, in order to be close to the horizontal resolution (1° × 1°) of JAMSTEC (see above), we use the night-time monthly averages SST map (1° × 1°) from the AMSR-E version 7 SSTs (see www.remss.com). The TAO array shows AMSR-E to have very small biases ($-0.03\,°C$) and STD ($0.41\,°C$) (Gentemann et al., 2010).

3.7.2   JAMSTEC data

As in Tang et al. (2014), we use a monthly gridded data set of global oceanic temperature on 1° × 1° grid processed and delivered by the Japan Agency for Marine-Earth Science and Technology (JAMSTEC) (Hosoda et al., 2010). This product is derived from the use of the optimal interpolation (OI) method that builds the gridded fields from ARGO floats, TRITON, and available CTD.

The temperature values at 10 m depth from INDO12 are used to compare with the first level of JAMSTEC salinity at 10 dbar ($\sim$ 10 m depth).

3.7.3 Results

Compared to both datasets, SST in the model is globally too warm (Fig. 19). The
SST bias is larger in the SCS where the influence of SCSTF is important (Qu et al., 2006) through the Luzon Strait. Positive biases are quite equivalent between the two datasets and are mainly located in the Pacific region. This increased the confidence in the positive bias in the SCS and corroborates the negative bias in the SSS. A too weak deep-water overflow in the Luzon strait can also explained this large bias. Zhao
et al. (2014) show that enhanced mixing in the SCS is a key process responsible for the density difference between the Pacific and SCS, which in turn drives the deep circulation in the Luzon Strait.

There is only one important region where the INDO12 SST is significantly too cold, it is in the south Indian Ocean. The negative bias relative to JAMSTEC is larger than
the bias relative to AMSR-E as it is for the RMSD (Fig. 20). It is localized in the Eastern Gyral Current (EGC) that flows eastward near 15° S, i.e., in the same region where a positive SSS bias exist (see previous section). In the Indonesian Archipelago, the SST bias relative to AMSR-E is slightly positive excepted in the Flores and Molluca seas and in the Timor passage where the bias is slightly negative. The Timor pas-
sage is the only region where a non-correlated bias exists between the two datasets (Fig. 21a). It still corresponds to the maximum of the temperature interpolation errors (Fig. 21b) in JAMSTEC. The temporal correlation (Fig. 20) is rather high everywhere and consistent between two datasets. Only one region located near the Halmahera eddy and along the SEC seems less correlated.

4 Summary

The INDESO operational system has been designed to monitor the evolution of the circulation, biogeochemistry and fish population dynamics within the Indonesian seas. Practically, INDESO addresses the needs of the Balitbang KP for a complete new
5 oceanographic centre in Perancak, Bali, from the building to the computer systems, the satellite antenna, and the transfer of expertise to the Indonesian experts. Since mid-September 2014, the entire system (Ocean, Biogeochemistry and Fish population dynamics) is fully operational in Perancak (see http://www.indeso.web.id) and deliver 10 day forecast/two weeks hindcast on a weekly basis. In order to validate the ocean
10 physic, the INDO12 model based on NEMO 2.3 was integrated during 7 years (2007–2013).

Globally, the mean circulation induced by the main equatorial and coastal currents (i.e., NGCC, SEC, NECC, SJC etc.) is well reproduced by the INDO12 ocean model. Excepted in coastal regions, EKE from INDO12 and EKE derived from altimeter data
15 share the same patterns. Model estimations of complex elevation amplitudes (amplitude and phase) agreed reasonably well with the TOPEX/POSEIDON, JASON 1 and JASON2 crossover observations, with better agreement for the diurnal constituents K1 than the semidiurnal constituent M2. A power-spectrum analysis of hourly SSH from Tide gauges and from simulated moorings shows that the model is in very good agree-
20 ment with the observations at low frequencies. It confirms that tides are a dominant forcing in the area, and that the tidal current is dominated by the diurnal (O1 and K1) and semidiurnal (M2 and S2) frequencies. Non-linear constituents (higher harmonics) contain less energy in the INDO12 model than the observations due to a lesser accuracy of non-linear processes near the coast.
25 The relative volume transport in the three major outflow passages in the INDO12 simulation is very close to one calculated from the INSTANT estimates. There is still an unbalance between the Timor strait (too strong) and the Ombai strait (too weak). The LST is Westward but still too weak. It could be due to the model resolution and

to the accuracy of the topography in the Philippine archipelago as suggested by Hulburt et al. (2011). In a recent study, Zhao et al. (2014) argue that an increase of the diapycnal diffusivity in the deep SCS and Luzon Strait enhances the transport of the deep circulation. A strong discrepancy exists between few existing measurements and the INDO12 simulation in the Lifamatola strait. As for the LST, it might be attributed to the bathymetry located upstream of the strait but also to the prescribed ocean forcing fields given by the Operational Ocean Forecasting System at 1/4° (PSY3V3R3). This could also explain the fact that the total transport in INDO12 is lower. Note also that INSTANT estimates and simulated INDO12 volume transports are not calculated over the same period (different ENSO signals).

The model is forced by explicit tides, which is able to generate part of the total internal tides energy. Accordingly to Niwa and Hibiya (2011), only 60 % of baroclinic energy can be generated with a 1/12° model. The model is also forced by an existing parameterization of the mixing (Koch-Larrouy et al., 2007). The resulting vertical mixing is able to erode the South and North Pacific subtropical waters salinity maximum as seen in the TS diagrams. Compared to climatologies, the inflow coming from North Pacific seems too salty for NPSW and too fresh in surface for NPIW, the inflow coming from South Pacific seems too salty and too warm in surface and sub-surface. The SPSW salinity maximum is strongly eroded from its entrance in the Halmahera Sea and vanishes in the Seram Sea. A too fresh surface water mass coming from the SCS throughflow and also a too strong mixing in the Banda Sea could explain a strong surface freshening into the Timor water masses. Nevertheless, an inter-annual variability exists depending on the year.

Compared to data collected during the INDOMIX cruise, a too strong vertical mixing occurs in the INDO12 model into the Halmahera sea which is not able to reproduce the observed wiggles and step features in the thermocline. On the other hand, TS profiles fit quite well in Banda sea and Ombai strait. Finally, all T/S diagrams in the Indonesian Archipelago show that the parent model has definitively not enough efficient vertical

mixing and that a higher resolution model including explicit tides is needed to well mix Pacific waters in the Indonesian Archipelago.

Compared to WOD (2013) in-situ data in the Luzon strait and in the SCS, the INDO12 model tends to be fresher mainly at surface.

⁵ We show that monthly SSS from space (Aquarius V3.0) and from an in-situ product (JAMSTEC) are quite consistent. This proves that the INDO12 model SSS is too low in the SCS and it corroborates the too weak volume transport of thermocline waters observed at Luzon strait. A positive bias exists in the Indian Ocean (95° E–15° S) where a smaller correlation between both INDO12 and both dataset exist. It is certainly due

¹⁰ to a systematic bias in the Eastern boundary conditions to a lesser accuracy of MDT.

Compared to two different SST dataset, one from space (AMSR-E) and one from an in-situ product (JAMSTEC), a global warm bias exists and is quite equivalent between the two datasets. It is consistent with the SSS bias. Stronger values of SST biases are located in the SCS and only one region is too cold, it is in the south Indian Ocean.

¹⁵ In the Indonesian Archipelago, it is difficult to discern a general trend due to large interpolation errors and lack of data.

We need to improve the large discrepancy in the SCS both for SSS and SST that are influenced both locally by the monsoons and remotely by the SCSTF/ITF. As mentioned by Qu et al. (2009), despite considerable progress that has been made in the

²⁰ past years, our understanding of the SCSTF is far from complete. They also pointed out that Mindoro strait can plays a significant role by shifting the NEC bifurcation (Mindanao Eddy) and then the Kurushio intrusion. This enhances the importance to have realistic Pacific open boundary conditions that necessarily influence the position of the Mindanao Eddy.

²⁵ Zhao et al. (2014) show that enhanced mixing in the SCS is a key process responsible for the density difference between the Pacific and SCS, which in turn drives the deep circulation in the Luzon Strait.

Different possible ways of the INDO12 model improvement can be suggested. A recent and better tidal forcing (FES 2012), see Carrere and Lyard (2012) could improve

tidal currents. New boundary conditions from the 1/12° global ocean forecasting model are also planned and should be more consistent (same horizontal resolution and same bathymetry). They could give us some indications of the Mindanao Eddy influence on the LST. Next developments should also include an improved bathymetry in major straits (entrance and exit). A specific study on vertical mixing induced by internal waves is necessary in order to improve the current tidal mixing parameterization.

Finally, although the ITF has a major impact on the global ocean circulation and climate variability, there are still too few measurements in the Indonesian Archipelago.

References

Alford, M. H., Peacock, T., MacKinnon, J. A., Nash, J. D., Buijsman, M. C., Centuroni, L. R., Chao, S.-Y., Chang, M.-H., Farmer, D. M., Fringer, O. B., Fu, K.-H., Gallacher, P. C., Graber, H. C., Helfrich, K. R., Jachec, S. M., Jackson, C. R., Klymak, J. M., Ko, D. S., Jan S., Johnston, T. M. S., Legg, S., Lee, I.-H., Lien, R.-C., Mercier, M. J., Moun, J. N., Musgrave, R., Park, J.-H., Pickering A. I., Pinkel, R., Rainville, L., Ramp, S. R., Rudnick, D. L., Sarkar, S., Scotti, A., Simmons, H. L., St Laurent, L. C., Venayagamoorthy, S. K., Wang, Y.-H., Wang, J., Yang, Y. J., Paluszkiewicz, T., and Tang, T.-Y. D.: The formation and fate of internal waves in the South China Sea, Nature, 521, 65–69, doi:10.1038/nature14399, 2015.

Barnier, B., Madec, G., Penduff, T., Molines, J.-M., Treguier, A.-M., le Sommer, J., Beckmann, A., Biastoch, A., Boning, C., Dengg, J., Derval, C., Durand, E., Gulev, S., Remy, E., Talandier, C., Theetten, S., Maltrud, M., McClean, J., and de Cuevas, B.: Impact of partial steps and momentum advection schemes in a global circulation model at eddy permitting resolution, Ocean Dynam., 56, 543–567, doi:10.1007/s10236-006-0082-1, 2006.

Boyer, T. P., Antonov, J. I., Baranova, O. K., Coleman, C., Garcia, H. E., Grodsky, A., Johnson, D. R., Locarnini, R. A., Mishonov, A. V., O'Brien, T. D., Paver, C. R., Reagan, J. R.,

Evaluation of an operational ocean model for the Indonesian seas – Part 1

B. Tranchant et al.

Full Screen / Esc

Printer-friendly Version

Interactive Discussion

Seidov, D., Smolyar, I. V., and Zweng, M. M.: World Ocean Database 2013, edited by: Levi-tus, S. and Mishonov, A., NOAA Atlas NESDIS 72, 209 pp., 2013.

Carrère, L., Lyard, F., Cancet, M., Guillot, A., and Roblou, L.: FES2012: a new global tidal model taking advantage of nearly 20 years of altimetry, in: Proceedings of meeting, 20 years of altimetry, Venice-Lido, Italy, 24–29 September 2012, 6 pp., 2012.

Castruccio, F. S., Curchitser, E. N., and Kleypas, J. A.: A model for quantifying oceanic transport and mesoscale variability in the Coral Triangle of the Indonesian/Philippines Archipelago, J. Geophys. Res.-Oceans, 118, 6123–6144, doi:10.1002/2013JC009196, 2013.

Dai, A. and Trenberth, K. E.: Estimates of freshwater discharge from continents: Latitudinal and seasonal variations, J. Hydrometeorol., 3, 660–687, 2002.

Dee, D. P., Uppala, S. M., Simmons, A. J., Berrisford, P., Poli, P., Kobayashi, S., Andrae, U., Balmaseda, M. A., Balsamo, G., Bauer P., Bechtold, P., Beljaars, A. C. M., van de Berg, L., Bidlot, J., Bormann, N., Delsol, C., Dragani, R., Fuentes, M., Geer, A. J., Haimberger, L., Healy, S. B., Hersbach, H., Holm, E. V., Isaksen, L., Kallberg, P., Kohler, M., Matricardi, M., McNally, A. P., Monge-Sanz, B. M., Morcrette, J.-J., Park, B.-K., Peubey, C., de Rosnay, P., Tavolato, C., Thepaut, J.-N., and Vitart, F.: The ERA-Interim reanalysis: configuration and performance of the data assimilation system, Q. J. Roy. Meteor. Soc., 137, 553–597, doi:10.1002/qj.828, 2011.

Egbert, G. D. and Erofeeva, S. Y.: Efficient inverse modeling of barotropic ocean tides, J. Atmos. Ocean. Tech., 19, 183–204, 2002.

Fang, G., Susanto, R. D., Wirasantosa, S., Qiao, F., Supangat, A., Fan, B., Wei, Z., Sulis-tiyo, B., and Li, S.: Volume, heat, and freshwater transports from the South China Sea to Indonesian seas in the boreal winter of 2007–2008, J. Geophys. Res., 115, C12020, doi:10.1029/2010JC006225, 2010.

Ffield, A. and Robertson, R.: Temperature finestructure in the Indonesian Seas, J. Geophys. Res., 113, C09009, doi:10.1029/2006JC003864, 2008.

Gentemann, C. L., Wentz, F. J., Brewer, M., Hilburn, K. A., and Smith, D. K.: Passive microwave remote sensing of the ocean: an overview, in: Oceanography from Space, revisited, edited by: Barale, V., Gower, J. F. R., and Alberotanza, L., Springer, Heidelberg, 13–33, 2010.

Gordon, A. L.: Oceanography of the Indonesian Seas and their throughflow, Oceanography, 18, 14–27, doi:10.5670/oceanog.2005.01, 2005.

Title Page

Abstract | Introduction

Conclusions | References

Tables | Figures

◄◄ | ►►

◄ | ►

Back | Close

Full Screen / Esc

Printer-friendly Version

Interactive Discussion

Gordon, A. L., Giulivi, C. F., and Ilahude, A. G.: Deep topographic barriers within the Indonesian Seas, in: Physical Oceanography of the Indian Ocean during the WOCE Period, editetd by: Schott, F., Deep-Sea Res. Pt. II, 50, 2205–2228, 2003a.

Gordon, A. L., Susanto, R. D., and Vranes, K.: Cool Indonesian throughflow as a consequence of restricted surface layer flow, Nature, 425, 824–828, doi:10.1038/nature02038, 2003b.

Gordon, A. L., Sprintall, J., Van Aken, H. M., Susanto, R. D., Wijffels, S., Molcard, R., Ffield, A., Pranowo, W., and Wirasantosa, S., The Indonesian throughflow during 2004–2006 as observed by the INSTANT program, Dynam. Atmos. Oceans, 50, 115–128, doi:10.1016/j.dynatmoce. 2009.12.002, 2010.

Gordon, A. L., Huber, B. A., Metzger, E. J., Susanto, R. D., Hurlburt, H. E., and Adi, T. R.: South China Sea throughflow impact on the Indonesian throughflow, Geophys. Res. Lett., 39, L11602, doi:10.1029/2012GL052021, 2012.

Gutknecht, E., Reffray, G., Gehlen, M., Triyulianti, I., Berlianty, D., and Gaspar, P: Evaluation of an operational ocean model configuration at $1/12°$ spatial resolution for the Indonesian seas – Part 2: Biogeochemistry, Geosci. Model Dev. Discuss., 8, 6669–6706, doi:10.5194/gmdd-8-6669-2015, 2015.

Hsin, Y.-C., Wu, C.-R., and Chao, S.-Y.: An updated examination of the Luzon Strait transport, J. Geophys. Res., 117, C03022, doi:10.1029/2011JC007714, 2012.

Hurlburt, H. E., Metzger, E. J., Sprintall, J., Riedlinger, S. N., Arnone, R. A., Shinoda, T., and Xu., X.: Circulation in the Philippine Archipelago simulated by $1/12°$ and $1/25°$ Global HYCOM and EAS NCOM, Oceanography, 24, 28–47, doi:10.5670/oceanog.2011.02, 2011.

Jerlov, N. G.: Optical oceanography, American Elsevier Publ. Co., Inc., New York, 194 p., 1968.

Kartadikaria, A. R., Miyazawa, Y., Varlamov, S. M., and Nadaoka, K.: Ocean circulation for the Indonesian seas driven by tides and atmospheric forcings: comparison to observational data, J. Geophys. Res., 116, C09009, doi:10.1029/2011JC007196, 2011.

Kidd, C., Dawkins, E., and Huffman, G.: Comparison of precipitation derived from the ECMWF operational forecast model and satellite precipitation datasets, J. Hydrometeorol., 14, 1463–1482, doi:10.1175/JHM-D-12-0182.1, 2013.

Koch-Larrouy, A., Madec, G., Bouruet-Aubertot, P., Gerkema, T., Bessières, L., and Molcard, R.: On the transformation of Pacific Water into Indonesian throughflow water by internal tidal mixing, Geophys. Res. Lett., 34, L04604, doi:10.1029/2006GL028405, 2007.

Koch-Larrouy, A., Morrow, R., Penduff, T., and Juza, M.: Origin and mechanism of Subantarctic Mode Water formation and transformation in the Southern Indian Ocean, Ocean Dynam., 60, 563–583, 2010.

Lagerloef and the Aquarius team: Aquarius Salinity Validation Analysis, Aquarius Project Document: AQ-014-PS-0016, 18 February 2013.

Large, W. and Yeager, S.: Diurnal to decadal global forcing for ocean and sea-ice models: the data sets and ux climatologies. CGD Division of the National Center for Atmospheric Research, NCAR Technical Note, NCAR/TN-460+STR, 2004.

Lehodey, P., Senina, I., and Murtugudde, R.: A spatial ecosystem and populations dynamics model (SEAPODYM) – modeling of tuna and tuna-like populations, Prog. Oceanogr., 78, 304–318, 2008.

Lellouche, J.-M., Le Galloudec, O., Drévillon, M., Régnier, C., Greiner, E., Garric, G., Ferry, N., Desportes, C., Testut, C.-E., Bricaud, C., Bourdallé-Badie, R., Tranchant, B., Benkiran, M., Drillet, Y., Daudin, A., and De Nicola, C.: Evaluation of global monitoring and forecasting systems at Mercator Océan, Ocean Sci., 9, 57–81, doi:10.5194/os-9-57-2013, 2013.

Levier, B., Tréguier, A. M., Madec, G., and Garnier, V.: Free surface and variable volume in the NEMO code, MERSEA IP report WP09-CNRS-STR03-1A, 47 pp., 2007.

Madec, G.: NEMO ocean engine, Note du Pole de modélisation, Institut Pierre-Simon Laplace (IPSL), France, No 27 ISSN No 1288–1619, 2008.

Madec, G., Delecluse, P., Imbard, M., and Lévy, C.: OPA 8.1 Ocean General Circulation Model reference manual, Note du Pole de modélisation, Institut Pierre-Simon Laplace (IPSL), France, No 11, 91 pp., 1998.

Maraldi, C., Chanut, J., Levier, B., Ayoub, N., De Mey, P., Reffray, G., Lyard, F., Cailleau, S., Drévillon, M., Fanjul, E. A., Sotillo, M. G., Marsaleix, P., and the Mercator Research and Development Team: NEMO on the shelf: assessment of the Iberia–Biscay–Ireland configuration, Ocean Sci., 9, 745–771, doi:10.5194/os-9-745-2013, 2013.

Mayer, B., Damm, P. E., Pohlmann, T., and Rizal, S.: What is driving the ITF? An illumination of the Indonesian throughflow with a numerical nested model system, Dynam. Atmos. Oceans 50, 301–312, 2010.

McClain, C. R., Feldman, G. C., and Hooker, S. B.: An overview of the SeaWiFS project and strategies for producing a climate research quality global ocean bio-optical time series, Deep-Sea Res. Pt. II, 51, 5–42, 2004.

Title Page

Abstract | Introduction

Conclusions | References

Tables | Figures

◄ | ►

◄ | ►

Back | Close

Full Screen / Esc

Printer-friendly Version

Interactive Discussion

McPhaden, M. J., Busalacchi, A. J., Cheney, R., Donguy, J. R., Gage, K. S., Halpern, D., Julian, M. Ji, P., Meyers, G., Mitchum, G. T., Niiler, P. P., Picaut, J., Reynolds, R. W., Smith, N., and Takeuchi, K.: The Tropical Ocean-Global Atmosphere observing system: A decade of progress, J. Geophys. Res., 103, 14169–14240, 1998.

Menezes, V. V., Phillips, H. E., Schiller, A., Domingues, C. M., and Bindoff, N. L., Salinity dominance on the Indian Ocean Eastern Gyral current, Geophys. Res. Lett., 40, 5716–5721, doi:10.1002/2013GL057887, 2013.

Metzger, E. J., Hurlburt, H. E., Xu, X., Shriver, J. F., Gordon, A. L., Sprintall, J., Susanto, R. D., and van Aken, H. M.: Simulated and observed circulation in the Indonesian Seas: 1/12° global HYCOM and the INSTANT observations, Dynam. Atmos. Oceans, 50, 27–300, 2010.

Munk, W. and Wunsch, C.: Abyssal Recipes II: energetics of tidal and wind mixing, Deep-Sea Res., 45, 1976–2000, 1998.

Niwa, Y. and Hibiya, T.: Estimation of baroclinic tide energy available for deep ocean mixing based on three-dimensional global numerical simulations, J. Oceanogr., 67, 493–502, doi:10.1007/s10872-011-0052-1, 2011.

Oke, P. R., Griffin, D. A., Schiller, A., Matear, R. J., Fiedler, R., Mansbridge, J., Lenton, A., Cahill, M., Chamberlain, M. A., and Ridgway, K.: Evaluation of a near-global eddy-resolving ocean model, Geosci. Model Dev., 6, 591–615, doi:10.5194/gmd-6-591-2013, 2013.

Qu, T., Kim, Y. Y., Yaremchuk, M., Tozuka, T., Ishida, A., and Yamagata, T.: Can Luzon Strait Transport play a role in conveying the impact of ENSO to the South China Sea?, J. Climate, 17, 3643–3656, 2004.

Qu, T., Yan, D., and Hideharu, S.: South China Sea throughflow: a heat and freshwater conveyor, Geophys. Res. Lett., 33, L23617, doi:10.1029/2006GL028350, 2006.

Rio, M. H., Guinehut, S., and Larnicol, G.: New CNES-CLS09 global mean dynamic topography computed from the combination of GRACE data, altimetry, and in situ measurements, J. Geophys. Res., 116, C07018, doi:10.1029/2010JC006505, 2011.

Sanchez Gomez, E., Cassou, C., Hodson, D. L. R., Keenlyside, N., Okumura, Y., and Zhou, T.: North Atlantic weather regimes response to Indian-western Pacific Ocean warming: a multi-model study, Geophys. Res.Lett., 35, L15706, doi:10.1029/2008GL034345, 2008.

Saraceno, M., Strub, P. T., and Kosro, P. M.: Estimates of sea surface height and near-surface alongshore coastal currents from combinations of altimeters and tide gauges, J. Geophys. Res., 113, C11013, doi:10.1029/2008JC004756, 2008.

Shriver, J. F., Richman, J. G., and Arbic, B. K.: How stationary are the internal tides in a high-resolution global ocean circulation model?, J. Geophys. Res.-Oceans, 119, 2769–2787, doi:10.1002/2013JC009423, 2014.

Song, Q., Gordon, A. L., and Visbeck, M.: Spreading of the Indonesian throughflow in the Indian Ocean, J. Phys. Oceanogr., 34, 772–792, doi:10.1175/1520-0485(2004)0342.0.CO;2, 2004.

Sprintall, J. and Revelard, A.: The Indonesian throughflow response to Indo-Pacific climate variability, J. Geophys. Res.-Oceans, 119, 1161–1175, doi:10.1002/2013JC009533, 2014.

Sprintall, J., Wijffels, S., Gordon, A. L., Ffield, A., Molcard, R., Susanto, R. D., Soesilo, I., Sopaheluwakan, J., Surachman, Y., and van Aken, H. M.: A New International Array to Measure the Indonesian Throughflow: INSTANT, EOS Transactions, 85, 369–376, 2004.

Sprintall, J., Wijffels, S. E., Molcard, R., and Jaya, I.: Direct estimates of the Indonesian Throughflow entering the Indian Ocean: 2004–2006, J. Geophys. Res., 114, C07001, doi:10.1029/2008JC005257, 2009.

Sprintall, J., Wijffels, S. E., Molcard, R., and Jaya, I.: Direct evidence of the South Java Current sustem in Ombai Strait, Dynam. Atmos. Oceans, 50, 140–156, 2010.

Sprintall, J., Gordon, A. L., Koch-Larrouy, A., Lee, T., Potemra, J. T., Pujiana, K., and Wijffels, S. E.: The Indonesian seas and their role in the coupled ocean-climate system, Nat. Geosci., 7, 487–492, doi:10.1038/ngeo2188, 2014.

Stammer, D., Ray, R. D., Andersen, O. B., Arbic, B. K., Bosch, W., Carrère, L., Cheng, Y., Chinn, D. S., Dushaw, B. D., Egbert, G. D., Erofeeva, S. Y., Fok, H. S., Green, J. A. M., Griffiths, S., King, M. A., Lapin, V., Lemoine, F. G., Luthcke, S. B., Lyard, F., Morison, J., Müller, M., Padman, L., Richman, J. G., Shriver, J. F., Shum, C. K., Taguchi, E., and Yi, Y.: Accuracy assessment of global barotropic ocean tide models, Rev. Geophys., 52, 243–282, doi:10.1002/2014RG000450, 2014.

Susanto, R. D., Gordon, Q., and Zheng, A. L.: Upwelling along the coasts of Java and Sumatra and its relation to ENSO, Geophys. Res. Lett., 28, 8, 1599–1602, 2001.

Susanto, R. D., Mitnik, L., and Zheng, Q.: Ocean internal waves observed in the Lombok Strait, Oceanography, 18, 80–87, doi:10.5670/oceanog.2005.08, 2005.

Talley, L. D. and Sprintall, J.: Deep expression of the Indonesian throughflow: Indonesian intermediate water in the South Equatorial Current, J. Geophys. Res., 110, C10009, doi:10.1029/2004JC002826, 2005.

Tang, W., Yueh, S. H., Fore, A. G., Hayashi, A., Lee, T., and Lagerloef, G.: Uncertainty of Aquarius sea surface salinity retrieved under rainy conditions and its implication on the water cycle study, J. Geophys. Res.-Oceans, 119, 4821–4839, doi:10.1002/2014JC009834, 2014.

Tozuka, T., Qu, T., and Yamagata, T.: Dramatic impact of the South China Sea on the Indonesian Throughflow, Geophys. Res. Lett., 34, L12612, doi:10.1029/2007GL030420, 2007.

Ueki, I., Kashino, Y., and Kuroda, Y.: Observation of the current variations off the New Guinea coast including the 1997–1998 El Nino period and their relationship with Sverdrup transport, J. Geophys. Res., 108, 3243, doi:10.1029/2002JC001611, 2003.

Van Aken, H. M. and Brodjonegoro, I. S.: IndraJaya, the deep-water motion through the Lifamatola passage and its contribution to the Indonesian throughflow, Deep-Sea Res. Pt. I, 56, 1203–1216, 2009.

Zeng, L., Liu, W. T., Xue, H., Xiu, P., and Wang, D.: Freshening in the South China Sea during 2012 revealed by Aquarius and in situ data, J. Geophys. Res.-Oceans, 119, 8296–8314, doi:10.1002/2014JC010108, 2014.

Zhao, W., Zhou, C., Tian, J., Yang, Q., Wang, B., Xie, L., and Qu, T.: Deep water circulation in the Luzon Strait, J. Geophys. Res.-Oceans, 119, 790–804, doi:10.1002/2013JC009587, 2014.

Evaluation of an operational ocean model for the Indonesian seas – Part 1

B. Tranchant et al.

Title Page

Abstract | Introduction

Conclusions | References

Tables | Figures

◄ | ►

◄ | ►

Back | Close

Full Screen / Esc

Printer-friendly Version

Interactive Discussion

Table 1. Sill depths (m) of the key straits and passages in the Indonesian seas from the scientific litterature and those used in INDO12.

Straits or passages	Observed estimate	INDO12
Inflow passages		
Sanhigihe Ridge (divides Pacific Ocean and Sulawesi Sea)	1350[a]	1250
Makassar Strait (Dewakang sill)	680[a]	675
Halmahera Sea Passages	580[a]	551
Lifamatola Passage	1940[b]	1950
Outflow passages		
Lombok strait	300[a]	200
Strait between Alor and Atauro Islands (upstream of Ombai strait)	1450[d]	1400
Wetar Strait (upstream of Ombai strait)	2450[c]	2050
Sumba Strait (north of Sumba Island)	900[d]	800
Savu Strait (connection between Savu Sea and Indian ocean)	1150[d]	1100
Timor passage (southern end)	1890[d]	1800

Source for sill depths: [a] Gordon et al. (2003a), [b] van Aken et al. (1988), [c] Sprintall et al. (2010), [d] Sprintall et al. (2009).

Table 2. Mean volume transport in the ITF (Sv and Ratio) for Lombok strait, Ombai strait and Timor passages. Mean values from INSTANT (2004–2006) and from the INDO12 simulation (2008–2013).

Straits	INSTANT (2004–2006)		INDO12 (2008–2013)	
	Sv	%	Sv	%
Lombok	2.6	17,3	2.07	16.7
Ombai	4.9	32,7	2.76	22.2
Timor	7.5	50	7.58	61.1
Total	15		12.41	

Full Screen / Esc

Table 3. Location of moorings during the INDOMIX campaign.

Mooring name	Longitude	Latitude
S0	129°59.08′ E	00°58.15′ N
S1	129°10.45″ E	00°03.63′ N
S2	128°52.99″ E	00°45.10′ S
S3	128°45.78″ E	01°08.13′ S
S4	126°59.88′ E	06°17.13′ S
S5a	125°23.14′ E	08°14.98′ S
S5b	125°14.64′ E	08°17.03′ S
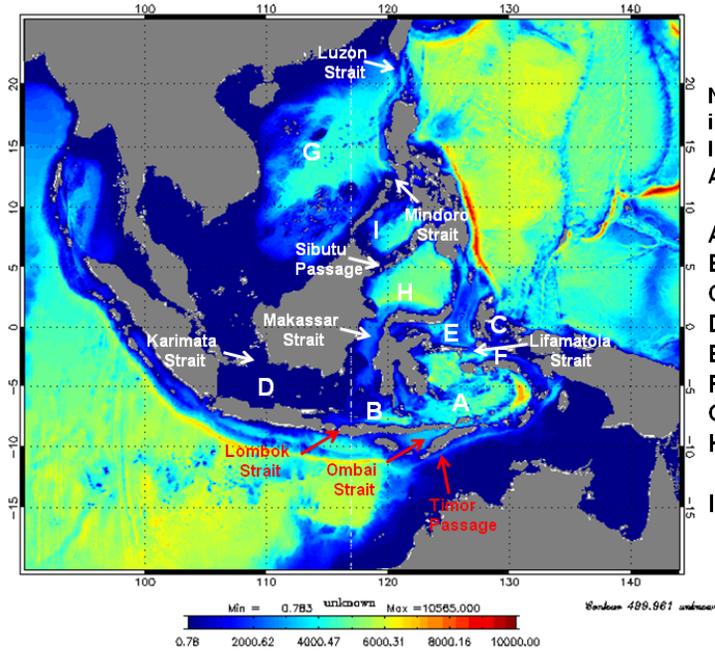
Names of main interior seas of the Indonesia Archipelago:

A: Banda
B: Flores
C: Halmahera
D: Java
E: Molluca
F: Seram
G: South China
H: Sulawesi or Celebes
I: Sulu

Figure 1. Bathymetry (meter) of the INDO12 configuration (Latitudes: 20° S–25° N and longitudes: 90–145° E). (ETOPOV2g/GEBCO1 + in-house adjustments in straits of major interest.) Three ITF exits are written in red. Main straits/passages are written in white.
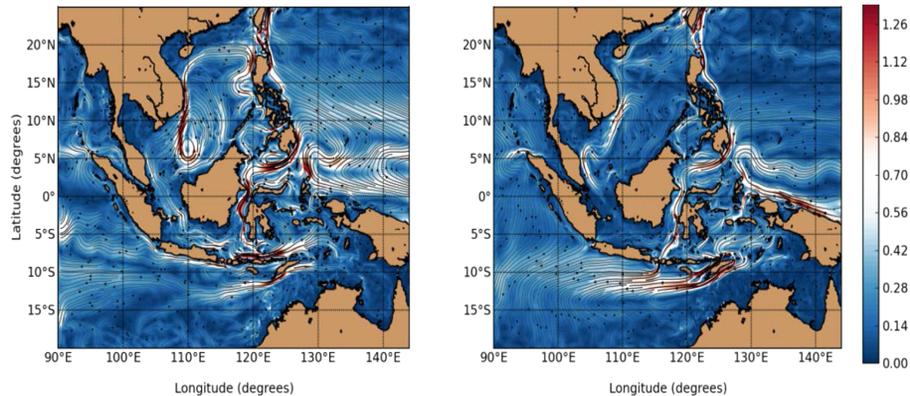
Figure 2. Mean Circulation at surface (16 m depth) during Boreal winter or DJF (left) and Boreal summer or JJA (right) during the 2008–2013 period.
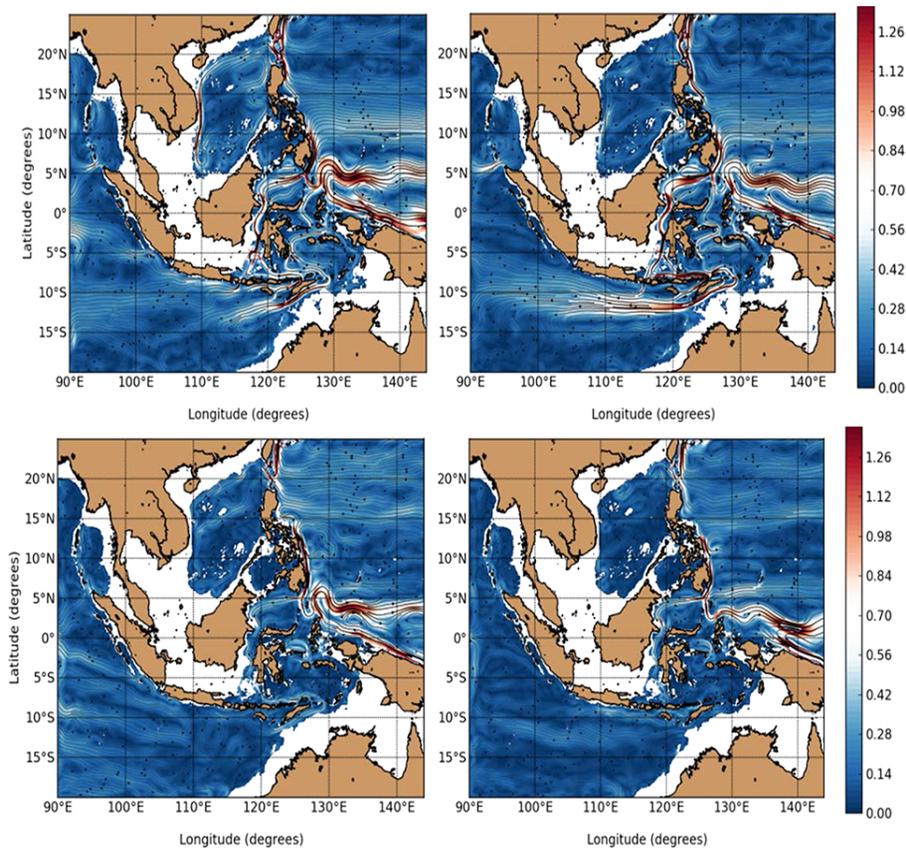
Figure 3. Mean Circulation at 100 m (up) and 300 m (bottom) during Boreal winter or DJF (left) and Boreal summer or JJA (right) during the 2008–2013 period.
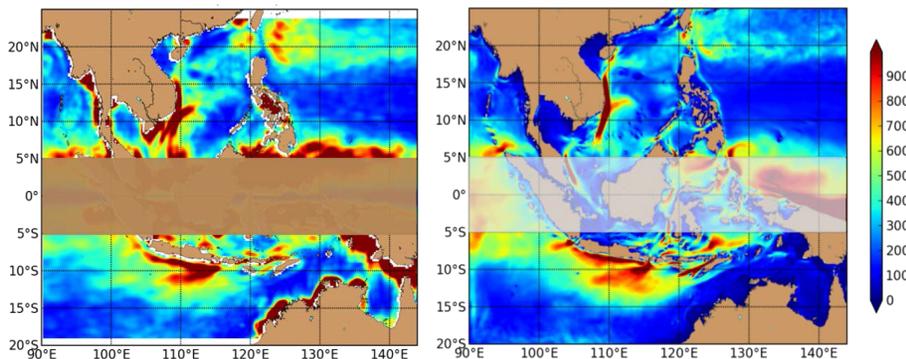
Figure 4. Mean EKE derived from altimetric data (AVISO products) (left) from INDO12 (right) for 2010–2013 period. EKE from altimetry is not reliable within a band of 5° on either side of the equator due to geostrophic approximation.

Title Page

Abstract | Introduction

Conclusions | References

Tables | Figures

|◄ | ►|

◄ | ►

Back | Close

Full Screen / Esc

Printer-friendly Version

Interactive Discussion
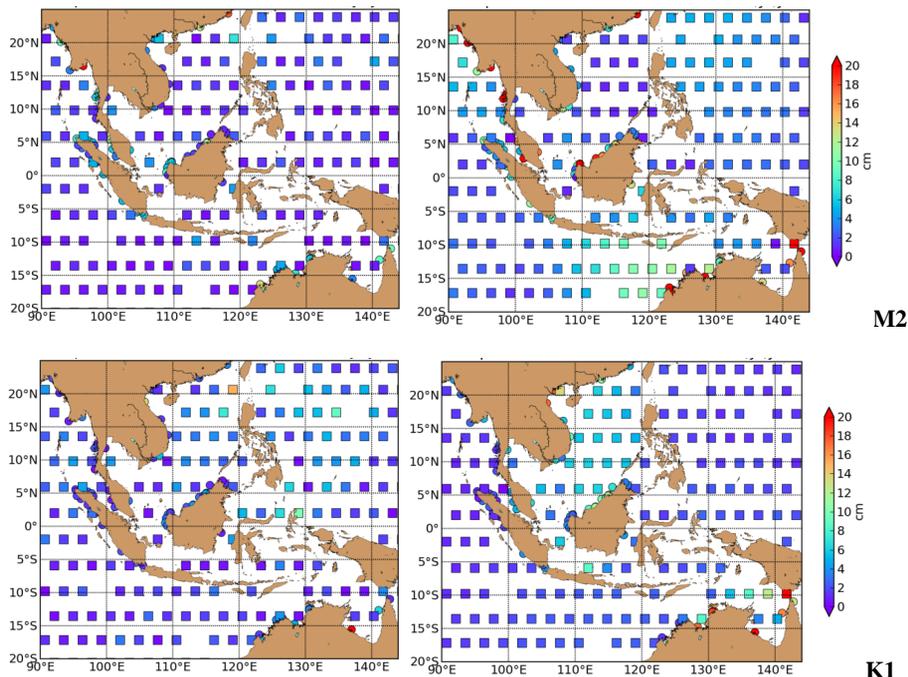
Figure 5. Surface tidal elevation differences (amplitude and phase) between at crossing points between TPX/J1/J2 and FES2012 (left) and INDO12 (right) symbolized by squares. Surface tidal elevation differences (amplitude and phase) between tide gauges and FES2012 (left) and INDO12 (right) symbolized by circles. Units are in cm. M2 (top) and K1 (bottom) tidal components.
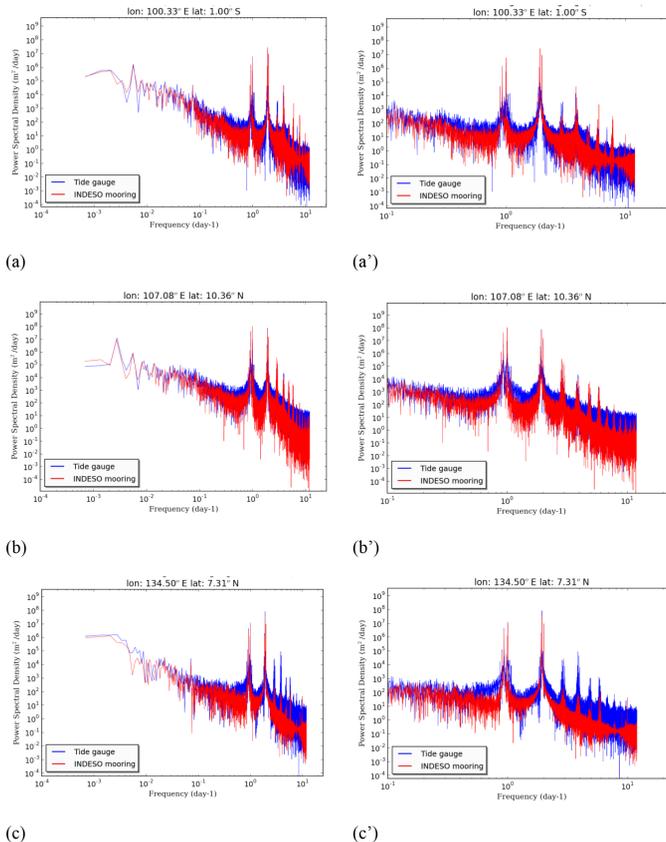
Figure 6. Power spectral density of the SSH for the model (red solid line) and for Tide gauges (blue solid line) at different locations (**a**: Padang (East-Sumatra), **b**: Vung Tau (SCS/South Vietnam) and **c**: Malakal (Pacific)) calculated during 2009–2012 period. Right panel is a zoom of the left panel.

Title Page

Abstract   Introduction

Conclusions   References

Tables   Figures

|◄   ►|

◄   ►

Back   Close

Full Screen / Esc

Printer-friendly Version

Interactive Discussion
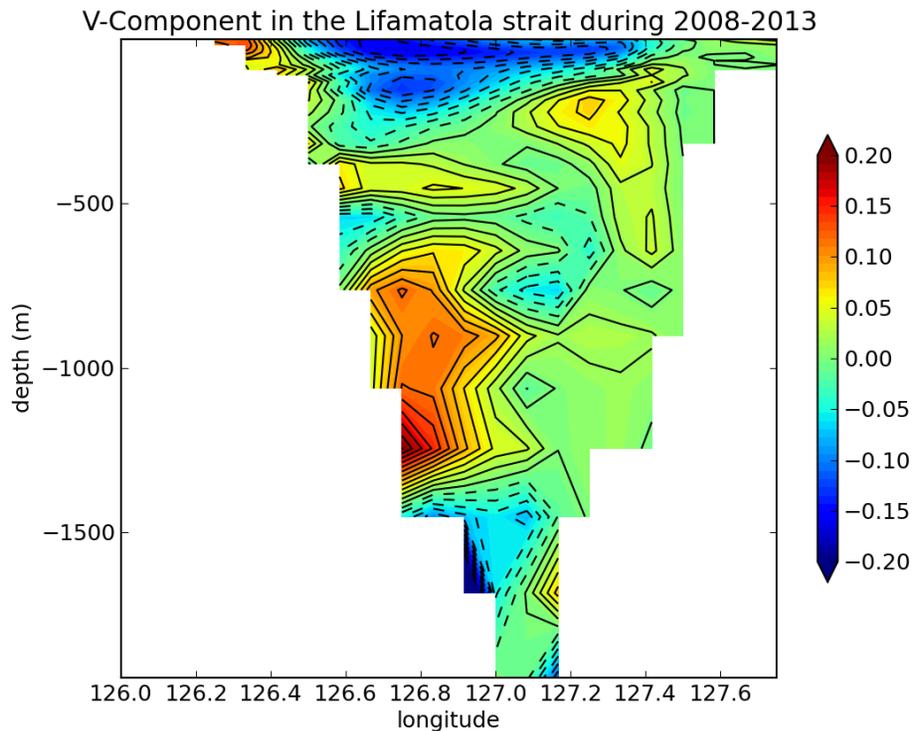
Figure 7. Mean of the along-strait velocity in the Lifamatola Strait (2008–2013). Contour (dashed lines) means a negative value (Southward flow). Contour (solid lines) means a positive value (Northward flow).

Title Page

Abstract | Introduction

Conclusions | References

Tables | Figures

|◄ | ►|

◄ | ►

Back | Close

Full Screen / Esc

Printer-friendly Version

Interactive Discussion
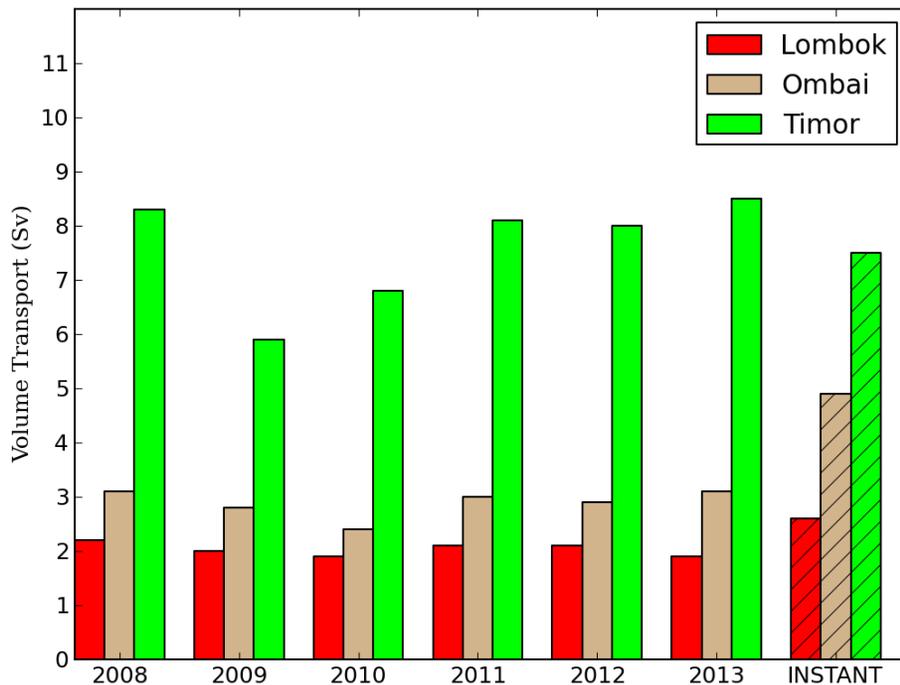
Figure 8. Model volume transport (Sv) into 3 main exits: Lombok (red), Ombaï (Braun), Timor (green) at different years. The Instant estimates (2004–2006) are shaded.
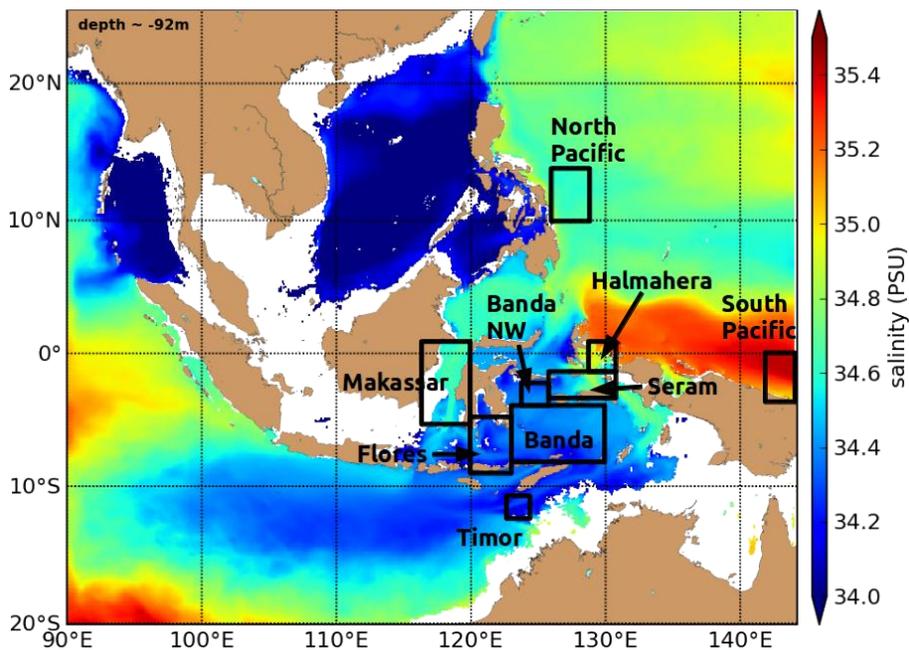
Figure 9. Main areas of water masses transformation.

Title Page

Abstract | Introduction

Conclusions | References

Tables | Figures

|◄ | ►|

◄ | ►

Back | Close

Full Screen / Esc

Printer-friendly Version

Interactive Discussion

Figure 10. T/S diagrams from INDO12 simulation (green line) averaged on the Pacific North area **(a)** and the South Pacific area **(b)** and compared to climatologies WOA 2009 (dotted line) and PSY3V3R3 (yellow) in 2012. Salinity (PSU) and Temperature (°C) respectively along x and y axes.

Halmahera   Seram   Banda

Makassar   Flores   Timor
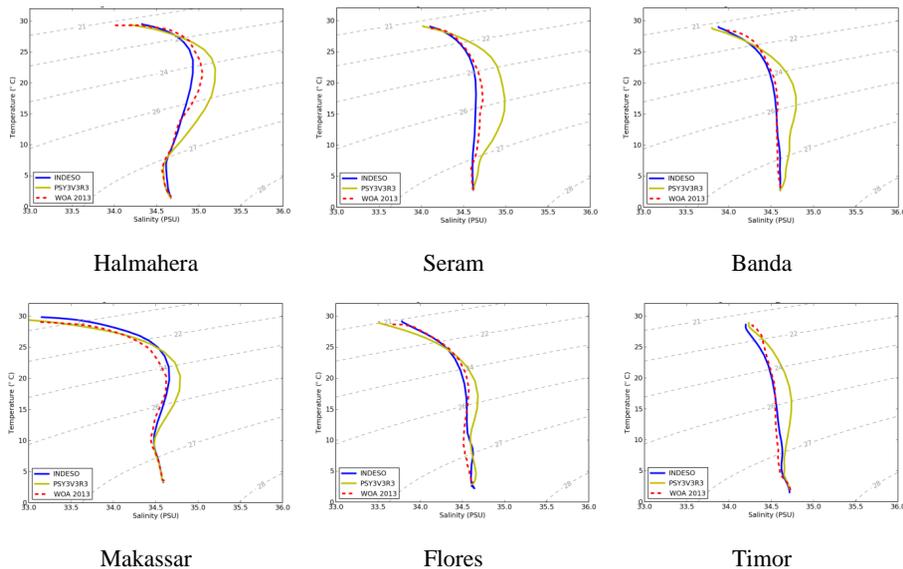
Figure 11. T/S diagrams from INDO12 simulation (blue line) averaged on different areas, Halmahera, Seram, Banda sea, Flores sea and Timor passage compared to climatologies WOA 2013 (red dotted line) and PSY3V3R3 (green line) for the 2008–2013 period. Salinity (PSU) and Temperature (°C) respectively along x and y axes.

Figure 12. T/S diagrams from INDO12 simulation (blue line) averaged on the Timor region and compared to climatologies WOA 2013 (red dotted line) and PSY3V3R3 (yellow line) for years 2008 to 2013. Salinity (PSU) and Temperature ($^\circ$C) respectively along x and y axes.

Full Screen / Esc

Figure 13. T/S diagrams from INDO12 simulation (dark blue dots) averaged blue line) area and from the parent model (PSY3) (yellow line) compared to INDOMIX data in July 2010 (red dots) at all locations. Salinity (PSU) and Temperature (˚C) respectively along x and y axes.

(a)

(b)

Figure 14. (a) Map showing the localization (red rectangle) and the number of profiles (8) in the area. **(b)** Collocated T–S diagrams to in-situ data (blue) from INDO12 simulation (red) and from climatology WOA2009 (yellow) in the Luzon strait (01 October–31 December 2013). Salinity (PSU) and Temperature (°C) respectively along x and y axes.

Title Page

Abstract | Introduction

Conclusions | References

Tables | Figures

|◄ | ►|

◄ | ►

Back | Close

Full Screen / Esc

Printer-friendly Version

Interactive Discussion

(a)

(b)
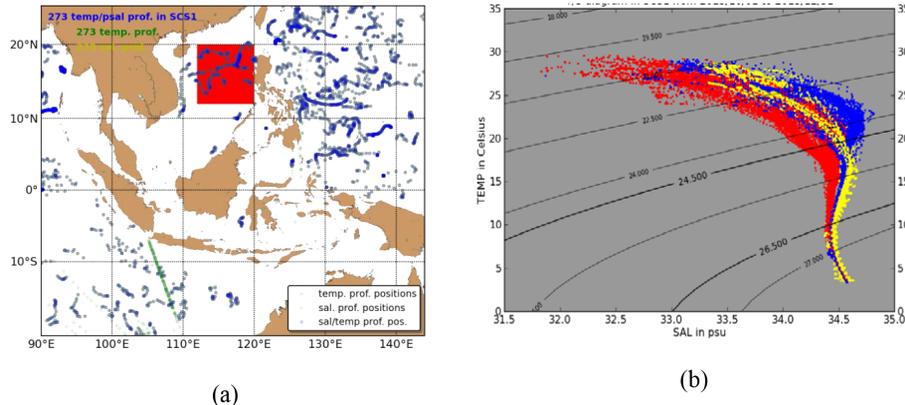
Figure 15. (a) Map showing the localization (red rectangle) and the number of profiles (273) in the area. **(b)** Collocated T–S diagrams to in-situ data (blue) from INDO12 simulation (red) and from climatology WOA2009 (yellow) in the SCS (01 October–31 December 2013). Salinity (PSU) and Temperature (°C) respectively along x and y axes.
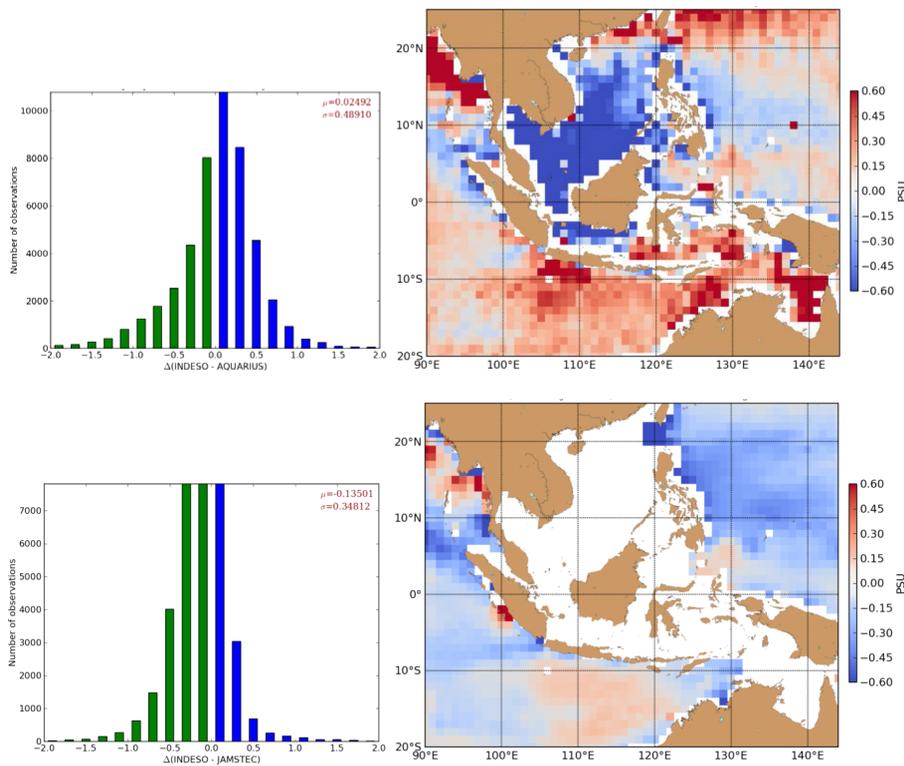
Figure 16. Comparisons between SSS collocated observations (monthly mean SSS) and INDO12 from August 2011 to December 2013: Aquarius L3 (V3.0) (top) and ARGO (JAM-STEC) (bottom).

mean correlation = 0.579   mean correlation = 0.607
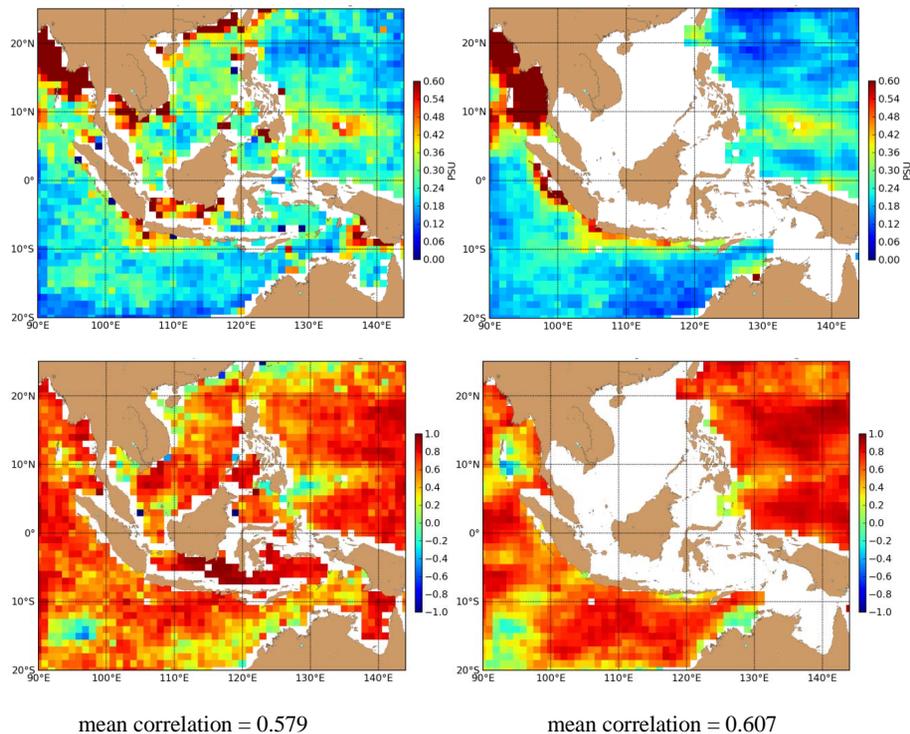
Figure 17. RMSD (top) and correlation (bottom) of INDO12 with respect to Aquarius (left) and JAMSTEC (right) monthly map from August 2011 to December 2013.
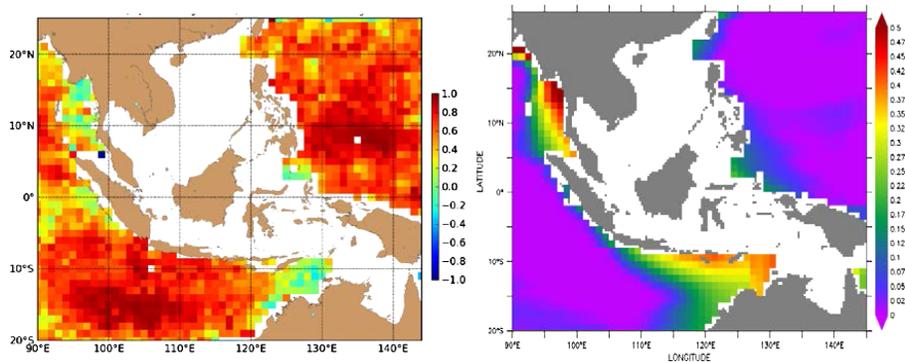
Figure 18. Mean temporal correlation between the (INDO12-Aquarius) bias and the (INDO12-JAMSTEC) bias and salinity interpolation error of JAMSTEC calculated from August 2011 to December 2013.

Full Screen / Esc

Printer-friendly Version

Interactive Discussion
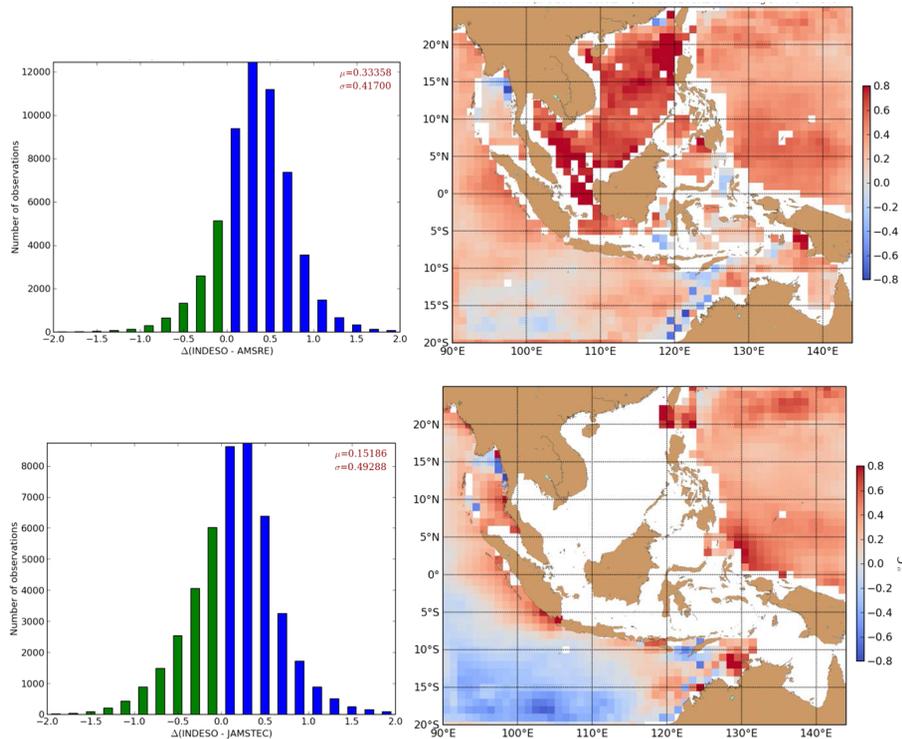
Figure 19. Comparisons between SST collocated observations (Monthly mean SST) and INDO12 for the years 2008–2010 (°C): AMSR-E (V7.0) (top) and ARGO (JAMSTEC) (bottom).
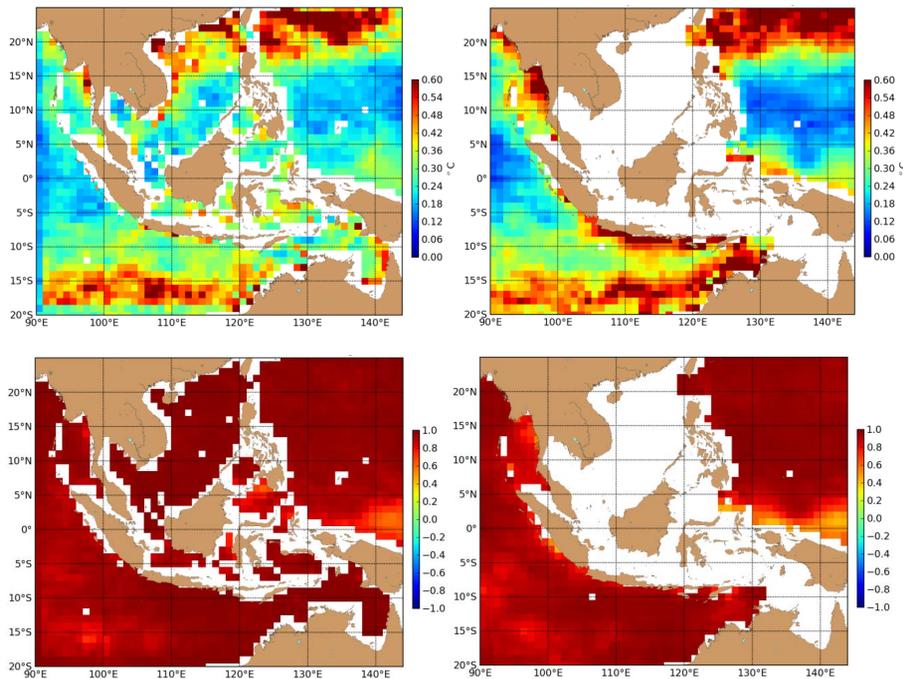
Figure 20. RMSD (top) and correlation (bottom) of INDO12 with respect to AMSR-E (left) and JAMSTEC (right) monthly map (2008–2010).
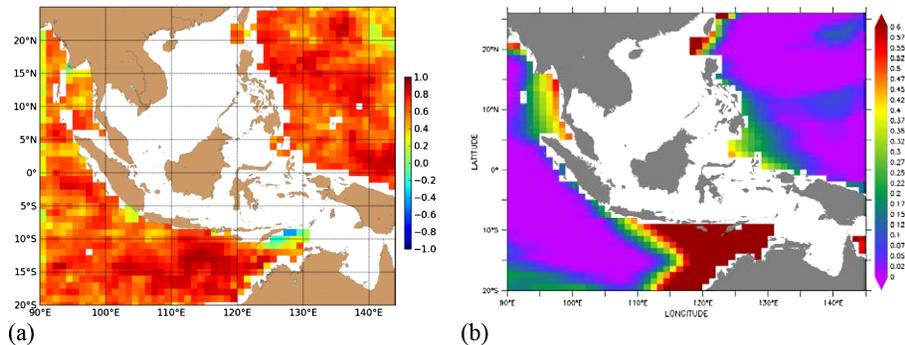
Figure 21. Mean temporal correlation between the (INDO12-AMSR-E) bias and the (INDO12-JAMSTEC) bias **(a)** and temperature interpolation error of JAMSTEC **(b)** calculated from 2008 to 2010.

Full Screen / Esc

Printer-friendly Version

Interactive Discussion